

The Rise of Graphene Photonic Crystal Fibers

Xu Zhou,* Qingyan Deng, Wentao Yu, Kaihui Liu,* and Zhongfan Liu*

2D graphene with tremendous novel properties is an ideal material for optical and optoelectronic applications. Meanwhile, photonic crystal fibers (PCFs) have been recognized as next-generation optical fibers that possess a designable porous structure, rich functions, and different working mechanisms. Recently, the integration of graphene with a PCF has formed a new hybrid fiber, a graphene photonic crystal fiber (Gr-PCF), which exhibits an extremely strong and tunable light–matter interaction across a broadband spectrum range and opens up a new interdisciplinary research direction. In this review, recent studies on, and achievements in graphene-traditional fibers and Gr-PCFs have been summarized from the aspects of the development process, preparation method, and device application. First, the graphene properties and the development and characteristics of PCFs are introduced. The discussion is continued with the existing fabrication technologies for hybrid graphene-traditional fibers. Next, the chemical vapor deposition method for Gr-PCFs is elaborated. Then, fiber devices based on graphene-traditional fibers, Gr-PCFs, and other 2D material fibers are presented. To conclude, challenges and perspectives are presented to encourage advanced Gr-PCF study.

thickness, including a strong light–matter interaction; a broadband light response; uniform light absorption across the visible and near-infrared (IR) spectrum; easy electro–optic tunability; strong optical nonlinearity; high transparency, electrical conductivity, tensile strength, and thermal conductivity; and chemical and environmental stability (Figure 1).^[6–20] This incredible breadth of properties allows graphene to be a valuable and useful nanomaterial, with most of the demand arising from research on and development of semiconductors, electronics, optics, optoelectronics, and composites.^[17–33] Especially with the rapid development of growth technology, the successful preparation of high-quality and large-scale single-crystal graphene has further stimulated people's enthusiasm for developing graphene toward practical applications.^[34–47]

Optical fibers have been developed into the foundation of today's information

communication technology since they were first experimentally realized in 1966.^[48] Beyond normal optical fibers, photonic crystal fibers (PCFs) with rich designable porous structures and functions have been one of the most important advances in optical fiber history since they were first fabricated in 1996.^[49–56] Benefiting from the designable structures and special working principles, PCFs exhibit many exotic properties, such as the ability to be filled, endless single-mode transmission,^[50,57–60]

1. Introduction

As the most famous 2D material, graphene has been the hot-spot and frontier of multidisciplinary research since it was first discovered in 2004.^[1–5] Due to the quantum confinement of electrons in 2D space and the absence of interlayer interactions, graphene has a unique linear electronic band structure and many distinctive characteristics irrespective of the atomic

X. Zhou, Q. Deng
Guangdong Provincial Key Laboratory of Quantum
Engineering and Quantum Materials
School of Physics and Telecommunication Engineering
South China Normal University
Guangzhou 510006, China
E-mail: xuzhou2020@m.scnu.edu.cn


W. Yu
Institute of Interdisciplinary Physical Sciences
School of Science
Nanjing University of Science and Technology
Nanjing 210094, China

K. Liu
State Key Laboratory for Mesoscopic Physics
Frontiers Science Center for Nano-optoelectronics
School of Physics
Peking University
Beijing 100871, China
E-mail: khliu@pku.edu.cn

K. Liu
International Centre for Quantum Materials
Collaborative Innovation Centre of Quantum Matter
Peking University
Beijing 100871, China

Z. Liu
Center for Nanochemistry (CNC)
Beijing Science and Engineering Center for Nanocarbons
Beijing National Laboratory for Molecular Sciences
College of Chemistry and Molecular Engineering
Peking University
Beijing 100871, China
E-mail: zfliu@pku.edu.cn

Z. Liu
Beijing Graphene Institute (BG1)
Beijing 100095, China

 The ORCID identification number(s) for the author(s) of this article can be found under <https://doi.org/10.1002/adfm.202202282>.

DOI: 10.1002/adfm.202202282

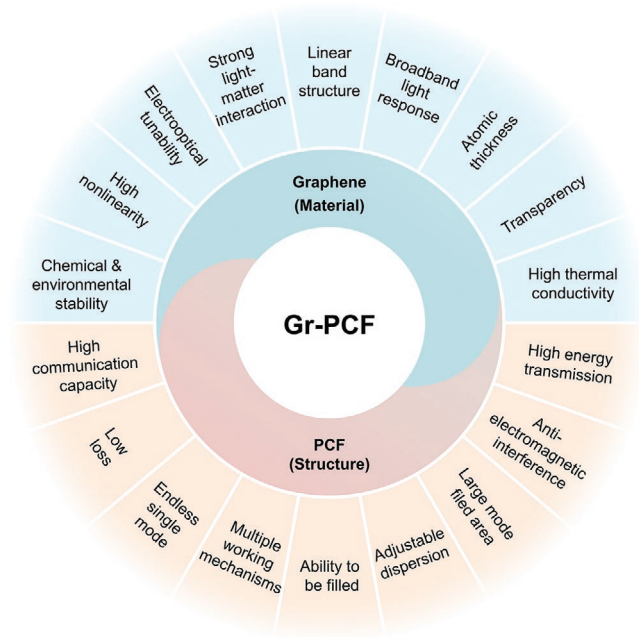


Figure 1. Concept diagram of a Gr-PCF with tremendous distinctive characteristics of graphene and a PCF. The integration of graphene and PCFs perfectly combines the structural properties of PCFs and the material properties of graphene, resulting in the new material of a Gr-PCF.

tunable dispersion,^[61–64] high birefringence,^[65,66] controllable large effective mode area,^[67,68] the photonic bandgap effect,^[69] high-power transmission,^[70,71] and low loss^[72–77] (Figure 1). Currently, PCFs have become a frontier hotspot providing new opportunities for optical and optoelectronic fiber devices, including all-optical switches, optical wavelength converters, dispersion compensators, supercontinuum light sources, and sensors.^[78–85]

Driven by the development and extremely valuable potential applications of graphene and optical fibers, they have been naturally combined into a new hybrid fiber (called a graphene optical fiber, Gr-optical fiber) and developed into various novel functional devices, which opens up a new interdisciplinary research direction (Figure 1). In the early stages of development, Gr-optical fibers used the traditional optical fiber with graphene on its end face and tapered or side-polished optical fibers with graphene on the exposed area of the fiber core, realized by the transfer methods.^[86,87] Those hybrid graphene fibers attract a lot of attention that are developed into various prototype fiber devices including pulse fiber lasers, fiber polarizers, fiber modulators, and fiber sensors. However, these Gr-optical fibers inevitably sacrifice the integrity of the fiber structure and transmission mode and exhibit a limited light–graphene interaction strength due to their limited interaction area size. With the development of graphene growth technology on nonmetallic materials, a graphene photonic crystal fiber (Gr-PCF) produced by the chemical vapor deposition (CVD) growth method was realized for the first time in 2019, where graphene films were grown on the air hole walls of a PCF (Figure 2).^[88] Such a combination not only avoids the destruction of the fiber structure and transmission mode but also can achieve an unlimited light–graphene interaction strength by adjusting the fiber length.

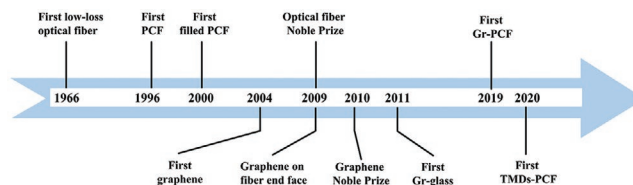


Figure 2. Chronological overview of the breakthroughs in the field of Gr-PCFs. All events are recorded according to their publication time. The abbreviation TMDs represents transition metal dichalcogenides.

In this review, we systematically describe the research results for Gr-PCFs and related Gr-optical fibers. We first summarize the basic properties of graphene, and the progress in optical fibers and the hybrid Gr-optical fiber. The discussion is continued with the existing fabrication technologies for hybrid graphene-traditional optical fibers. Next, the CVD growth method for Gr-PCFs is particularly reviewed. Then, the device applications of graphene-traditional fibers, Gr-PCFs, and related 2D material-PCFs with attractive performance are presented in detail. Finally, we discuss the challenges and opportunities for Gr-PCFs and provide our vision on future perspectives and conclusions in this field. This review will hopefully help obtain a deep understanding and boost the advancement of Gr-PCF research.

2. The Concept of a Graphene Optical Fiber

2.1. The Properties of Graphene

Graphene, a real 2D material made of a single layer of carbon atoms arranged in a hexagonal lattice, has certainly been one of the most important discoveries in the 21st century since it was discovered in 2004.^[1–4] It is widely called a “super material” for its unique and fascinating structural and physical properties with incredible breadth, which allow it to play a significant role in a vast number of products, processes, and industries and have great application potential in semiconductors, electronics, optics, electro–optics, and composites.^[17–37]

Graphene is the thinnest object ever created, with a one carbon atom thickness of ≈ 0.34 nm, and is arranged in a honeycomb lattice structure (a carbon–carbon bond length of 1.42 Å and a lattice parameter of 2.46 Å) (Figure 3a). It has strong sp^2 carbon–carbon covalent bonding within the layer and weak interlayer bonding via the van der Waals force, allowing it to slide and dissociate quite easily. It is the strongest material ever tested, with an intrinsic tensile strength of ≈ 130 GPa and a Young’s modulus (stiffness) close to 1 TPa, which is ≈ 100 times stronger than steel with the same thickness.^[89,90] It exhibits an exceptionally high in-plane thermal conductivity of up to $\approx 5 \times 10^3$ W mK⁻¹,^[91,92] which is extremely suitable for high-performance electronics and optoelectronics because keeping the operating temperatures low is imperative. It shows surprising chemical and environmental stability (theoretical melting point as high as ≈ 5000 K).^[93–95] It is hydrophobic unless subjected to surface treatment, such as oxygen plasma, and apparently impermeable to most liquids and gases.^[96]

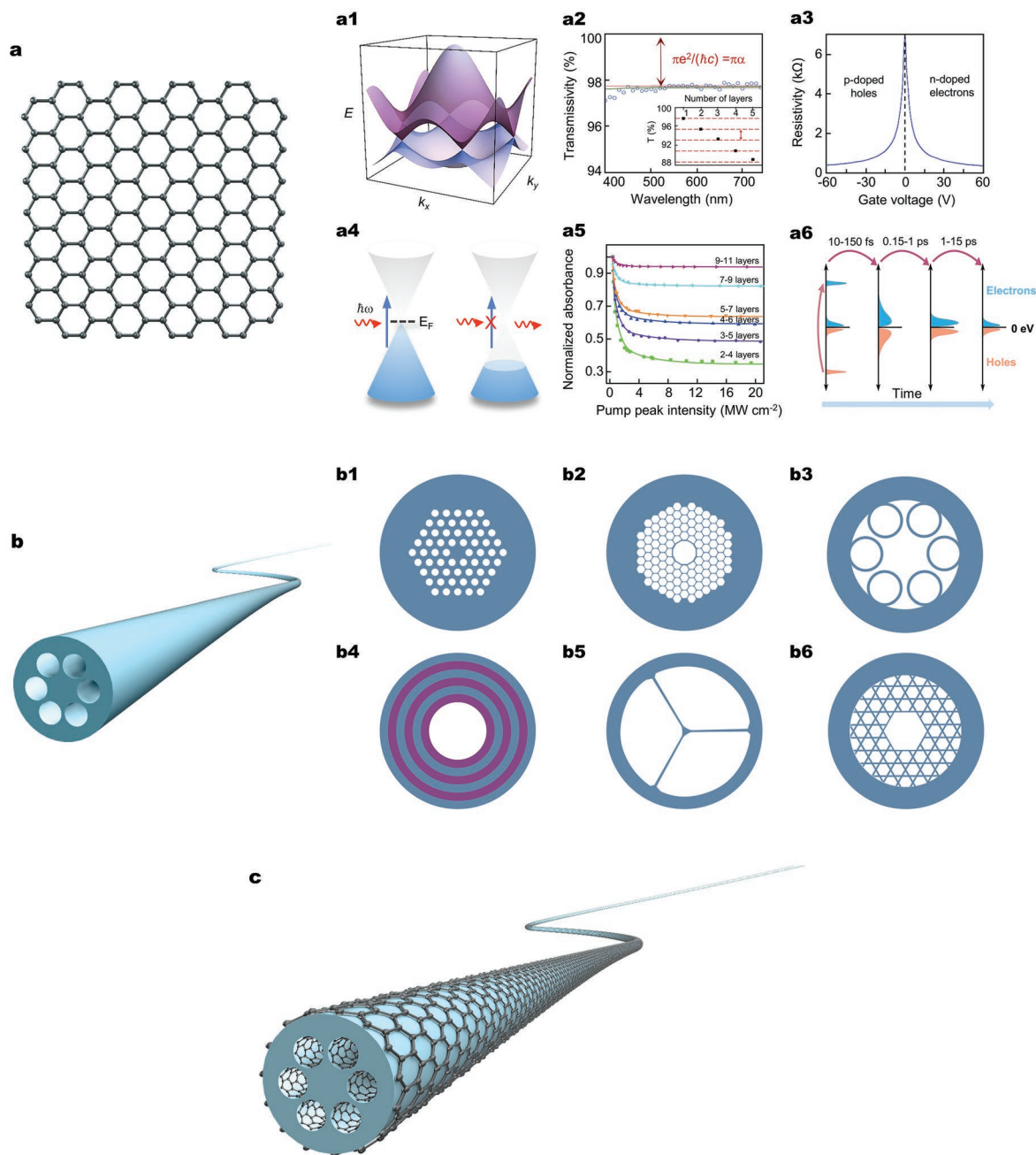


Figure 3. Schematic of graphene along with the basic properties and PCFs with different cross-sectional patterns. a) Atomic structure of 2D graphene with a honeycomb lattice. a1) Electronic band structure of graphene. Linear dispersion relation showing the vertically mirrored Dirac cones intersecting at the Fermi energy. a2) Uniform absorbance of 2.3% for graphene across the visible and near-IR spectrum for vertically incident light, where the absorption coefficient is precisely defined by $\pi\alpha \approx 2.3\%$, and α is the fine-structure constant. Inset: light absorption linearly increases with the number of layers. a3) Typical resistivity as a function of gate voltage for graphene, showing the ambipolar nature as the conduction switches between the hole (left) and electron (right) regimes, separated by the charge neutrality (Dirac) point where the resistance reaches its maximum. a4) Modulation of the light absorption of graphene by Fermi level shifting. Graphene does not absorb a photon with an energy of $\hbar\omega$ when $\hbar\omega/2 < |E_F|$ due to the Pauli blocking effect in the conduction band or empty energy level in the valence band. a5) Graphene exhibits an evident saturable absorption effect, in which the light absorptivity decreases with increasing incident light intensity. a6) Schematic of the likely processes by which optically excited, nonequilibrium electron and hole distributions approach equilibrium. After excitation, the distribution rapidly thermalizes and cools within 10–150 fs. Hot carriers cool further due to intraband phonon scattering within 0.15–1 ps. Electrons and holes relax to the equilibrium distribution after 1–15 ps. b) Structure schematic of a PCF with wavelength-scale air holes periodically arranged around the core. The cross-sectional patterns of common representative PCFs are those of the b1) total internal reflection PCF, b2) photonic bandgap PCF, b3) antiresonant HCF, b4) Bragg fiber, b5) suspended core PCF, and b6) Kagome HCF. c) Structure schematic of a Gr-PCF with a graphene film covering the outside surface and the inner hole walls. a1) Reproduced with permission.^[7] Copyright 2009, American Physical Society. a2) Reproduced with permission.^[6] Copyright 2008, AAAS. a3) Reproduced with permission.^[3] Copyright 2007, Nature Publishing Group. a5) Reproduced with permission.^[19] Copyright 2009, Wiley-VCH. a6) Reproduced with permission.^[20] Copyright 2008, American Chemical Society.

Due to the quantum confinement of electrons and the absence of interlayer interactions, graphene has a unique electronic structure with a linear energy dispersion relation, resulting in a series of extraordinary electrical and optical properties that differ from those of conventional materials. The electron of graphene exhibits zero effective mass with a high Fermi velocity of $\approx 10^6$ m s⁻¹ ($\approx 1/300$ the speed of light) near the Dirac point,^[97–100] which means an unprecedented very large carrier mobility and highly efficient electrical conduction capability along the 2D plane (Figure 3a1).^[7] Specifically, the resistivity is very low, ≈ 1.0 $\mu\Omega$ cm⁻¹, which is slightly smaller than that of silver (≈ 1.5 $\mu\Omega$ cm⁻¹).^[101] The carrier mobility is up to $\approx 10^6$ cm² V s⁻¹ at liquid-helium temperature (≈ 4 K),^[102] $\approx 0.6 \times 10^6$ cm² V s⁻¹ at liquid-nitrogen temperature (≈ 77 K),^[103] and $\approx 0.2 \times 10^6$ cm² V s⁻¹ at room temperature (≈ 300 K) due to the weak electron–phonon interaction for the suspended film.^[104–106] These are crucial properties for high-speed electronics and optoelectronics.

The photonic properties of graphene are equally remarkable. Despite being only a single atomic layer thick, graphene exhibits a surprisingly strong light–matter interaction, with a uniform and high absorbance of $\approx 2.3\%$ across the visible and near-IR spectrum for vertically incident light, where its absorption coefficient is precisely defined by $\pi\alpha \approx 2.3\%$, with $\alpha \approx 1/137$ being the fine-structure constant (Figure 3a2).^[6,107] Because each graphene sheet in few-layer graphene can be seen as a 2D electron gas with little perturbation from the adjacent layers, the optical absorption was experimentally demonstrated to be proportional to the number of layers of few-layer graphene, with each layer absorbing 2.3% over the visible spectrum and with only 0.1% reflectivity for the monolayer, which rises to $\approx 2\%$ for ten layers.^[6,107–109]

Owing to its unique linear band structure, graphene can interact with light from the ultraviolet to far-IR and even to the terahertz and microwave regions, and the electronic transition and corresponding optical response (carrier concentration, electrical conductivity, resistance, light absorption, reflectivity, refractive index, and other physical parameters) can be easily tuned by changing the Fermi level (E_F) through external electrical gating or chemical doping.^[22,26–33] Hence, graphene exhibits peculiar ambipolar behavior switched by an E_F shift or a gate voltage (Figure 3a3).^[3,12] E_F is determined by the carrier concentration $n = E_F^2 / (\pi\hbar^2 v_F^2)$, where π , \hbar , and v_F are the circular constant, reduced Planck's constant, and Fermi velocity, respectively. In a field-effect transistor (FET) configuration of graphene/SiO₂/doped-Si (or ionic-liquid/graphene), E_F can generally be shifted by hundreds of meV (or even up to 1.7 eV) by applying a gate voltage across a SiO₂ dielectric (or ionic liquid electrolyte layer). The doping concentration of carriers is typically less than 5×10^{12} cm⁻², which is limited by the breakdown of the SiO₂ layer, while electrolyte gating can induce carrier concentrations as high as 10^{14} cm⁻².^[110,111]

The light absorption of graphene can be easily electro–optically modulated, which follows the rules below (Figure 3a4). The interband transition only occurs above the threshold of $\hbar\omega/2 = |E_F|$ due to the zero bandgap, where incident photons have an energy of $\hbar\omega$ (ω is the angular frequency). In other words, graphene does not absorb a photon with an energy of $\hbar\omega$ (electron interband transition is forbidden) when $\hbar\omega/2 < E_F$ due to the Pauli blocking effect in the conduction band or

empty energy level in the valence band. Therefore, for slightly doped graphene ($|E_F| < \hbar\omega/2$), the high-frequency dynamic conductivity is dominated by the interband contribution for a wide bandwidth from visible to IR, which covers the telecommunication bands and the mid-IR region.^[109] Graphene can achieve large modulation of optical transitions of ≈ 2.3 eV or ≈ 540 nm (i.e., an E_F shift of $\approx \pm 1.15$ eV) by electrical gating, which is extremely rare,^[102] although field-effect-modulated electrical conductivity has long been the basis of modern electronics.^[11–18,22,112] Undoubtedly, graphene with such an excellent characteristic of a tunable optical response can be widely exploited for many novel optical and optoelectronic devices.

Graphene also exhibits strong nonlinearity associated with exceptionally high third-order susceptibility within the visible and near-IR spectral range, including saturable absorption and the Kerr effect. Graphene exhibits an evident saturable absorption effect in which the light absorptivity decreases with increasing incident light intensity (Figure 3a5).^[19–21] Compared to semiconductor saturable absorber mirrors (SESAMs, some of the most prevalent absorbers), graphene has an ultrashort recovery time (< 200 fs, that for SESAMs is approximately on the picosecond level), low saturable absorption (≈ 0.6 MW cm⁻¹,^[2] one order of magnitude lower than that of SESAMs), great relative modulation depth ($> 60\%$ per layer, two to three times larger than that of SESAMs), and wavelength-independent operation (ranging from visible to terahertz, SESAMs have narrowband operation of < 100 nm), allowing it to operate efficiently for the generation of broadband ultrafast laser pulses (Figure 3a5,a6).^[19–21,113–115] Under more intense laser illumination, graphene could also possess a nonlinear phase shift due to the optical Kerr effect, in which the refractive index variation is proportional to the local electric field of the light. It possesses a giant nonlinear Kerr coefficient of 10^{-13} – 10^{-7} m² W⁻¹ (the experimental results are related with the excitation source, sample preparation techniques, and substrate materials), almost nine orders of magnitude larger than that of bulk dielectrics.^[116–124] This suggests that graphene may be a powerful nonlinear Kerr medium with the possibility of observing a variety of nonlinear effects, the most important of which is the soliton.^[116–123]

The distinctive properties of graphene allow multiple functions of signal emission, transmission, modulation, and detection to be realized in one material, particularly alluring for a variety of device applications, such as high-frequency transistors,^[22] electron/light emitters,^[125] transparent electrodes,^[126] supercapacitors,^[15] broadband polarizers,^[28] tunable all-optical/electro–optical modulators,^[26,27] photodetectors,^[23–25] sensors,^[127] mode-locked/Q-switched fiber lasers,^[18] and terahertz generators,^[29,30] and so on.^[32,33] This incredible breadth of distinctive properties allows graphene to be a valuable and useful material, with most of the demand arising from research on and development of semiconductors, electronics, optics, optoelectronics, and composites. Graphene, as a new material, is said to have great potential to change the future, as in the case of the past history.

2.2. The Progress in Optical Fibers

An optical fiber provides the highest-quality optical waveguide for information communication and photon manipulation and

has been the hardware foundation of the information age since the first low-loss optical fiber was experimentally realized in 1966.^[48] Today's communication networks are mainly composed of single-mode and multimode silica fibers, typically including a solid core surrounded by a solid cladding material with a lower index of refraction. They can be fabricated into side-polished fibers or tapered-fibers where fiber core is exposed and the core-guided light can interact with other materials on the exposed area via evanescent field. Based on this characteristic, they have attracted intense attentions over the past several decades and found a lot of applications such as power couplers, sensors, and lasers.^[128–132]

From the late 20th century to the dawn of the 21st century, booming development of optical fiber technology was witnessed, especially the emergence of PCFs (also known as microstructured fibers or holey fibers). A PCF is an optical fiber with special structures, in which wavelength-scale air holes are periodically arranged around the core (Figure 3b, b1–b6). Compared with traditional optical fibers, PCFs have a completely different principle of light wave propagation, a designable porous structure, and rich functions, which has opened a new horizon for in-fiber manipulation of optical wavelengths, modes, dispersions, polarizations, and nonlinearities^[49–56] since such fibers were first fabricated in 1996 by Russell and his colleagues.^[49] The properties of a PCF are determined by its structure, and as fiber functions become increasingly prominent, PCF structures are being designed and fabricated according to their functionalization instead of the strict concept of photonic crystals. Until now, PCFs have been one of important progress in the optical fiber field and researched in various fields, such as by utilizing their ability to be filled, endless single-mode transmission,^[50,57–60] tunable dispersion,^[61–64] high birefringence,^[65,66] controllable effective mode area,^[67,68] photonic bandgap effect,^[69] high-power transmission,^[70,71] and low loss.^[72–77]

PCFs, according to their structures, can be simply divided into solid-core PCFs and hollow-core PCFs (HCFs).^[75] According to the light transmission mechanism, specific PCF categories include total internal reflection PCFs (or index-guiding PCFs, PCFs guiding light via a higher-index solid core with a lower-index cladding modified by the presence of air holes, Figure 3b1), photonic bandgap PCFs (PCFs that confine light through the photonic bandgap effect, Figure 3b2), antiresonant HCFs (some tubes surround an empty central region and form a hollow pipe that confines light following the antiresonance principle, Figure 3b3), and Bragg fibers (photonic bandgap fibers formed by concentric rings of a multilayer film and related to the Bragg effect Figure 3b4). In addition, common PCFs generally also include suspended core PCFs (a kind of index-guiding fiber with a suspended core, Figure 3b5) and Kagome HCFs (with an incomplete photonic bandgap, related to antiresonant reflection, Figure 3b6). The first PCF demonstrated in 1996 was a total internal reflection PCF with a solid core.^[49] The first photonic bandgap PCF was realized in 1998.^[51]

Due to the physical limit of Rayleigh scattering and the nonlinear Shannon limit, conventional silica single-mode optical fibers have little potential for further improvement.^[133] However, PCFs based on special structures and working mechanisms have great potential to achieve high energy transmission, low energy loss, and wide single-mode transmission

range for the applications of high-capacity communication and high-energy lasers. Among them, the endless single-mode PCFs (a kind of total internal reflection PCF with a solid core, Figure 3b1) can only support a single fundamental mode and have a large core diameter with a large mode area across the full wavelength band, which eliminates the special requirements for the core diameter of the traditional single-mode optical fiber.^[50,57] Its large mode area also means high energy delivery without material damage or other adverse effects caused by the fiber nonlinear properties. Indeed, a large mode area PCF with a mode field diameter larger than 26 μm has been commercially available and used for single-mode high power delivery,^[134] broadband multiwavelength transmission,^[49] etc. Compared to solid-core fibers, HCFs with guiding of light in an air core (ideally in a vacuum) have been extremely more appealing since their first realization in 1999^[52] because of their lower Rayleigh scattering, lower nonlinearity, lower transmission loss, and higher laser damage threshold in air holes.^[135–147] In 2018, an antiresonant HCF transmitted a high-power laser of up to ≈ 45 W average power.^[148] In 2020, a nested antiresonant nodeless fiber was demonstrated to achieve the current record loss of ≈ 0.28 dB km^{-1} at 1550 nm, while its theoretical loss limit is less than 0.1 dB km^{-1} , lower than that of the standard single-mode fiber.^[149–152]

An important feature of PCFs is their ability to act as a substrate capable of hosting novel functional materials (e.g., gases, liquids, and solids) inside their air holes. They are usually used as low-loss platforms with high aspect ratios and long interaction lengths to achieve some functions or devices with unique properties. 1) Gas-filled PCFs. Gas-filled HCFs offer unprecedented opportunities to observe novel nonlinear phenomena because they can provide the requirements of a high intensity at low power, a long interaction length, and a good quality transverse beam profile for efficient nonlinear processes. In addition, in a gas-filled PCF, the optical dispersion of the gas can be controlled by the pressure and gas species, which is vital in many types of nonlinear interactions, including supercontinuum generation, soliton-effect pulse compression, self-phase modulation, and four-wave mixing.^[153–157] For example, the first gas-filled HCF was reported in 2002, which demonstrated enhanced stimulated Raman scattering of hydrogen gas over a long interaction length of 1 m with an ultralow pulse laser energy for the first time.^[73] In 2013, a rare gas-filled Kagome HCF provided a simple, compact, and widely tunable ultraviolet source for the first time with a tunable 176–550 nm ultrafast pulse.^[155] 2) Liquid-filled PCFs. By varying the external temperature or electric field, the refractive index of fluids (e.g., liquid crystals) can be changed, which gives the possibility of controlling the optical properties of liquid-filled PCFs (such as the location of the bandgaps, thermo-optic coefficient, light intensity, and polarization states) so that they can be developed into sensors, switches, tunable bandpass filters, fiber probes, and so on.^[158] For example, the high-extinction-ratio optical bandgap position within 1300–1600 nm for a commercially available PCF filled with liquid crystals was thermally tuned from 20 to 80 °C, as reported in 2009.^[159] 3) Solid-filled PCFs. Solid functional materials (including metals, chalcogenide glasses, silicon, and germanium) can be filled or deposited in the air holes of HCFs by the pressure-assisted melt filling method or high-pressure CVD technique for the purpose of directly

functionalizing optoelectronic fibers. However, the melting temperature of target solid materials should be lower than that of a fused silica fiber of ≈ 400 °C, which greatly limits the choice of materials. Uniform film deposition over long fiber lengths and the probable destruction of the air hole pattern are remaining challenges for this task. For example, the integration of precisely doped semiconductor materials and high-quality rectifying semiconductor junctions into PCFs realized high-speed and up to 3 GHz bandwidth in-fiber functionalities in 2012.^[160] Selectively filling metal into some air holes brings inherently enhanced polarization-dependent transmission, which could eventually be used for the development of an in-fiber absorbing polarizer or notch filters.^[161–164]

The flexible structural designability, ability to fill air holes, and diversity of the working principles of PCFs result in disparate novel properties and wide application prospects in lasers, sensors, supercontinuum light sources, optical fiber communication systems, etc. beyond traditional fibers. With the emergence of new materials and the development of new technologies, an increasing number of new properties and applications will be developed for PCFs and hybrid PCFs, which will continue to be research hotspots in the future.

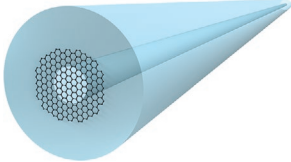
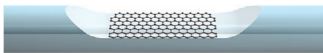

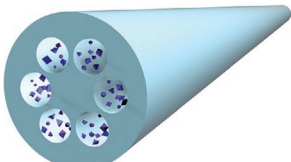
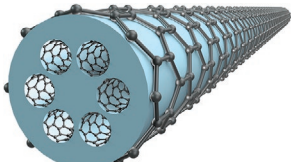
2.3. The Hybrid Graphene Optical Fibers

The integration of optical fibers with various functional materials has greatly expanded the functions and application regimes, directly leading to a new scientific research field (Figure 3c). The emergence of graphene provides a valuable opportunity for the development of optical fibers toward the multimaterial and multifunctional path. The integration of graphene and optical fibers can perfectly complement both advantages. On the one hand, the high-quality waveguide structure of an optical fiber can greatly enhance the light–graphene interaction. On the other hand, the novel optical properties of electrical tunability, broad spectral response, and saturable absorption effect of graphene can be endowed on optical fibers. Consequently, shifting the graphene E_F by applying an electric field or other means can manipulate the photons in the optical fiber, such as the intensity, phase, and polarization state, which results in many new all-fiber devices based on Gr-optical fibers, such as fiber polarizers,^[165] pulsed mode-locked fiber lasers,^[19,21,166–171] optical/electro-optic fiber modulators,^[88,172] and fiber sensors.^[173]

The combination of an optical fiber and graphene requires that graphene can interact with fiber core-guided light. Therefore, according to the structures of Gr-optical fibers, the combination methods can be summarized into four main categories, as shown below (Table 1).

- 1) The first and most intuitive method is attaching a graphene film onto the core position at the fiber end face so that the light transmitted in the fiber core can directly interact with graphene. Such a structure is easy to be realized where the graphene on fiber end face can maintain its high quality during the transfer process. As early as 2009, utilizing this method, Tang et al. for the first time exploited a 756 fs graphene-based ultrafast pulsed fiber laser with a 1.79 MHz repetition rate at 1565 nm.^[19] In 2010, Ferrari et al. sandwiched a graphene-polyvinyl alcohol mixture between two fiber connectors with a fiber adapter and developed a 713 fs, 19.9 MHz graphene-based mode-locked fiber laser at 1559 nm.^[21,174] However, this method suffers from an obvious drawback of a relatively weak light–graphene interaction as the result of the short interaction length of only nanometers when the beam directly passes through the graphene films. In addition, the direct penetration of graphene by a laser in the fiber cavity can easily lead to thermal damage of graphene, which is not conducive to the generation of high-energy mode-locked pulses.
- 2) Therefore, to improve the heat dissipation and the light–graphene interaction, the method of attaching graphene onto a side-polished optical fiber and a tapered optical fiber has been employed. The fabrication technology of transferring graphene onto side-polished and tapered optical fibers is relatively simple, so a number of works based on these Gr-optical fibers, including pulse fiber lasers and fiber polarizers, have emerged. For example, in 2010, Song et al. demonstrated graphene mode-locked fiber lasers with efficient laser pulsation and evanescent field interaction between the propagating light and graphene film sprayed onto the planar region of a side-polished fiber in the form of a graphene solution.^[166] In 2011, Loh et al. demonstrated the operation of a broadband Gr-optical fiber polarizer with an extinction ratio of 27 dB in the telecommunication band, in which a graphene film was transferred onto a side-polished optical fiber.^[165] In 2014, Tong et al. reported an ultrafast all-optical modulator at ≈ 1.5 μm with a response time of ≈ 2.2 ps, making use of a graphene-tapered optical fiber by the transfer method.^[170] Due to their simple and easy fabrication characteristics, these Gr-optical fiber-based devices have greatly promoted the development of hybrid graphene optical fibers.
- 3) The two methods above inevitably sacrifice the integrity of the fiber structure and transmission mode, which limits their development space and potential in turn. In particular, their light–graphene interaction strength cannot be further improved. Although the interaction between graphene and core-guided light can be enhanced by increasing the lateral dimension or longitudinal length of the core leakage area, this operation also results in more core-guided light field leaking into the air, which also leads to a decrease in the strength of the light–graphene interaction and an increase in the coupling loss. Therefore, finding a more reasonable way to realize a strong light–graphene interaction, under the premise of ensuring the structural integrity of the optical fiber, is necessary. The ideal way is to attach a graphene film onto the core surface of an original fiber. Some efforts have been made to attach graphene nanoparticles onto PCFs as a saturable absorber in mode-locked fiber lasers.^[167–171] However, this method still has insurmountable shortcomings; that is, the randomly distributed attachment of graphene nanoparticles and the introduced impurities can destroy the optical fiber transmission mode and optical transmission stability. These drawbacks were left as unsolved issues until 2019.^[88]
- 4) To date, the most effective integration is to grow graphene films onto the PCF hole walls that surround the core, which provides obvious and unique advantages: a) the atomic thickness of

Table 1. Comparison of different kinds of hybrid graphene optical fibers.

Configurations		Preparation method	Light–graphene interaction way	Interaction area/strength	Advantages	Drawbacks	Reference
Graphene on fiber end face		Transfer	Penetration	The core end face with about μm in diameter; Weak	Simple structure, easy preparation	Short interaction length of nanometers; graphene is easy to thermal damage. low preparation efficiency.	[19,21,174]
Gr-side-polished fiber		Transfer	Evanescent field	The exposed core region with about cm in length; Normal	Easy preparation	The cracks of graphene membrane, transfer-induced doping, wrinkles and surface contamination are inevitable; low preparation efficiency.	[165,166]
Gr-tapered fiber		Transfer	Evanescent field	The exposed core region with about cm in length; Normal	Easy preparation	The cracks of graphene membrane, transfer-induced doping, wrinkles and surface contamination are inevitable; low preparation efficiency.	[170]
Gr-PCF		Capillarity	Evanescent field, reflection or transmission	The core region with entire fiber length; Strong	Easy preparation, high preparation efficiency	The randomly distributed attachment of graphene nanoparticles and the introduced impurities	[167–169]
Gr-PCF		CVD	Evanescent field reflection or transmission	The core region with entire fiber length; Strong	Massive production, strong light–graphene interaction	Complicated preparation process; Difficult to control quality of graphene.	[88]

graphene keeps the PCF structure and main optical functions intact; b) an unlimited light–graphene interaction strength can be achieved by adjusting the fiber length. The idea was for the first time achieved with the CVD method by Liu and his team in 2019,^[88] which also demonstrated an efficient and nonharmful manufacturing strategy for mass production at the meter scale for Gr-PCFs. In contrast, those attempts mentioned above have only been accomplished on the micrometer scale and with a small interaction area and harmful effects on the fiber modes. Continuing in a similar way, they further realized in 2020, growth of the uniform 2D material MoS₂ along the entire PCF hole walls via a two-step CVD method, and the MoS₂-PCF showed strongly enhanced second- and third-harmonic optical generation of up to ≈ 300 times.^[175]

The different fabrication designs of hybrid Gr-optical fibers, including Gr-PCFs, have greatly advanced the development of multifunctional and multimaterial optical fibers, as well as graphene optoelectronic devices. In particular, the CVD growth strategy opens up a new direction for mass production of 2D-crystal-based all-fiber devices, targeting next-generation optical fibers with various new functionalities.

3. The Growth of Graphene Photonic Crystal Fibers

3.1. The Preparation of Graphene Traditional Fibers

Generally, the widely used methods for preparing Gr-traditional fibers are the wet transfer method and the dry transfer method.^[176,177] No liquid solvent is used in the dry transfer process, which is usually suitable for transferring small-area graphene, and the obtained graphene on fiber surface is high quality and less pollution. Liquid solvent is used in the wet transfer process which is usually suitable for the transfer of large-area graphene by CVD method, but it tends to introduce more impurities.

Here, we briefly describe the operation process of the wet transfer method by taking the graphene CVD-grown on copper foil transferred onto the fiber surface as an example. Because large-area self-supporting 2D materials cannot achieve, a widely used transfer medium, the polymethyl methacrylate (PMMA), is usually needed as the supporting layer. So, the first step is to spin-coat PMMA on the graphene on a copper foil. Second, the PMMA–graphene–copper foil is placed in

FeCl_3 solution or ammonium persulfate solution to chemically dissolve the copper foil, and then the PMMA–graphene film is left floating on the solution. Third, the PMMA–graphene film is carefully transferred to the target surface with tweezers, after PMMA–graphene film is rinsed with deionized water. Finally, the PMMA is dissolved and removed using alcohol or acetone vapor, and the remaining graphene is on the surface of the fiber. The PMMA, that is, transfer media, can be replaced by poly(lactic acid), poly(phthalaldehyde), and poly(bisphenol A carbonate). The wet transfer method is suitable for almost all 2D materials grown on substrate surfaces. But the membrane cracks, transfer-induced doping, wrinkles, as well as surface contaminations are usually inevitable.

The dry transfer method is usually used for the graphene on silicon substrates which is mechanically exfoliated from graphite by a tape. First, a small piece of polydimethylsiloxane (PDMS) with flat surface is fixed on a glass slide. Second, graphene is pasted on the PDMS surface. In a micropositioning system, the glass slide/PDMS/graphene and target substrate (optical fiber) are fixed on a multidimensional manipulator arm and a 4D translation stage, respectively. Third, under the microscope, graphene is precisely shifted to the target position and lowered to contact the optical fiber. Finally, after the glass slide is raised slowly by manipulator arm, the graphene film is left on the fiber surface due to the adhesion between the graphene and the target substrate is greater than that between the PDMS and graphene film. This method can obtain high-quality graphene on the target substrate, but it has low success rate, and the size of the transferred graphene is not controllable.

The transfer methods have their universal characteristics, but also suffer from some limitations of low efficiency and the inability to the inner surface of a target object (Table 1). And more efficient methods for fabricating graphene-optical fibers are in demand for a long time. The CVD method could be a good way to improve the efficiency of producing Gr-optical fibers. However, it is rarely reported yet, which is probably because the transfer method is simpler and of lower cost for a fiber device demo in labs so far.

3.2. The Growth of Graphene on Glass

Due to the advantages of low cost, simple preparation process, strong controllability, and mass production, together with the obvious catalytic effect of a metal substrate on graphene growth, the CVD method has become the mainstream method for the preparation of large-area, high-quality graphene on metal substrates and has been developed to a relatively mature stage.^[34–47,178–185] However, the CVD growth strategy of Gr-PCFs is challenging due to the lack of a metal catalyst and the difficulty in gas flow control along the long micrometer-sized holes in a silica PCF. The successful growth of Gr-PCFs benefits from extensive experience in the CVD growth of graphene glass/insulator substrates.^[186–196]

In the CVD growth of graphene, the substrate plays a crucial role, participating in the cracking process of the carbon source gas and the migration, nucleation, and growth process of carbon atoms in it. Therefore, the growth conditions and

difficulties required for the growth of graphene on different substrates are quite different. For example, the commonly used metal substrates (Cu, Ni, Pt, etc.) have an excellent catalytic cracking effect on carbon-containing molecules (such as methane, ethanol, and ethylene), and carbon atoms more easily migrate and nucleate in metal substrates; thus, graphene CVD-grown on metal substrates generally has a relatively high single crystallinity, a large size, and a faster growth rate. However, nonmetal substrates, including quartz, sapphire, borosilicate glass, and soda lime glass, have very weak catalytic performance, which makes carbon-containing source molecule cracking and carbon species migration on their surface difficult. Therefore, the nucleation and growth of graphene on a glass surface is difficult. As a result, graphene growth on a glass surface generally shows a lower growth rate and a poorer crystalline quality. Generally, under typical experimental conditions with the same methane precursor, CVD growth of graphene on glass takes over 1–7 h, while that of graphene on Cu foil takes only 10 min.^[189,190]

The temperature required for CVD growth of graphene is usually above 1000 °C. Therefore, under metal-catalyst-free growth conditions, carbon precursors (such as CH_4) undergo a thermochemical decomposition process rather than a metal-catalyzed cracking process.^[197,198] In this case, a higher temperature (1000–1120 °C) at atmospheric pressure is usually needed to promote more thorough methane decomposition (≈ 1000 °C thermal decomposition temperature) and produce higher concentrations of activated carbon species.^[199,200] Replacing methane with other carbon source gases of acetylene^[201,202] and alcohol^[203] can also improve the quality and growth rate of graphene because the relatively low decomposition temperatures of acetylene and alcohol result in a reduced growth temperature of graphene on dielectric substrates.

In general, increasing the temperature, changing the carbon source gas, varying the gas pressure, using plasma and metal remote assistance, etc. can achieve growth of graphene glass or improve the growth quality and production rate. These CVD growth strategies provide extensive experience for the preparation of Gr-PCFs.

3.3. The Growth of Graphene Photonic Crystal Fibers

The used PCF (index-guiding type) consisted of a solid silica core and a surrounding silica cladding region with four circles of air holes only ≈ 4 μm in diameter (Figure 4). Even when PCFs are made of silica, the CVD growth conditions and kinetics processes of Gr-PCFs are completely different from those of graphene glass in open space because graphene needs to be grown in the confined space of the fiber holes with micron-level diameters and meter-level lengths. Gr-PCFs are grown under the conditions of ≈ 1100 °C, at atmospheric or low pressure, with methane as the carbon feedstock. Graphene films are grown on both the outside surface and inside the hole walls of PCFs, which guarantees maintenance of the structural integrity. Because of the very weak catalytic effect of silica on cracking methane and the laborious migration of carbon atoms on the silica surface, graphene nucleation, and growth on silica surfaces generally exhibit lower growth rates and poorer crystalline quality. Consequently,

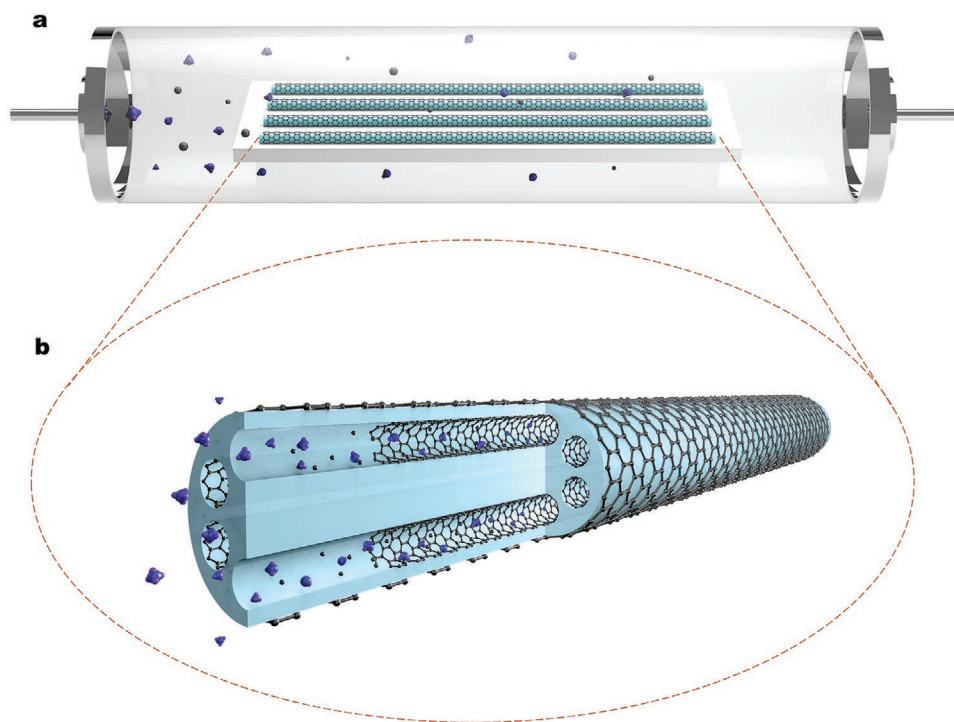


Figure 4. Schematic of Gr-PCF growth by the CVD method. a) Multiple meter-length PCFs placed in a muffle furnace with a quartz tube for mass CVD growth of Gr-PCFs under the conditions of a temperature above 1000 °C and methane as the carbon feedstock. b) Zoomed-in picture with a partial cutaway view of the upper figure. Methane molecules are cracked into various carbon source molecules. These particles enter the micron-sized air holes of the PCF and are then deposited, forming graphene.

graphene in PCFs is usually polycrystalline with a small domain size of ≈ 50 nm. However, the thickness can be controlled from one to ten layers by the growth time.

The atmosphere-pressure CVD and low-pressure CVD (pressure of 0.5–1.0 kPa) growth method can be used to produce different qualities. In atmosphere-pressure CVD, the graphene film thickness is increasing along the gas flow as a result of the increase in active carbon species during long-time thermal decomposition in downstream locations. In low-pressure CVD, graphene film with uniform thickness along the fiber axis is realized due to the uniform distribution of carbon active molecules when carbon source gas flows in the narrow fiber hole approaches a free molecular flow situation.

The CVD method achieves the Gr-PCF with length of up to 50 cm. It is convenient and more efficient that one can cut them into small sections for mass application because many Gr-PCF applications need only centimeter-length fibers.

4. The Application of Graphene Photonic Crystal Fibers

4.1. Graphene Traditional Fiber Devices

Motivated by the peculiar properties of the broadband working wavelength range, tunable light–matter interaction, and polarization-selective absorption, researchers have developed Gr-optical fibers into optical fiber polarizers, fiber lasers, and other fiber devices.

Most Gr-optical fiber polarizers are based on side-polished fibers, because the asymmetric coverage of graphene around the fiber core can expediently introduce the different attenuations of two orthogonal polarization modes by the polarization-selective absorption of graphene. The first Gr-optical fiber polarizer was achieved in 2011, where graphene film was transferred onto a side-polished fiber.^[165] Originated from the different attenuation of the TE and TM modes, the Gr-optical fiber polarizer exhibited TE-pass feature with an extinction ratio up to ≈ 27 dB at 1550 nm wavelength. In 2015, electrically manipulable all-fiber graphene polarizer and saturable absorber were demonstrated for the first time where randomly stacked multilayer graphene was used.^[204] In this tunable fiber polarizer, the graphene-based FET was built on a side-polished fiber with an ion-liquid dielectric, and the transmission of TM mode changes from 87.1% to 90.8% and TE mode shows a more drastic transmission change from 39.2% to 83.4% by gate-voltage adjusting from 0.7 to 1.8 V. Furthermore, the fiber polarizer was integrated into a fiber laser system as an electrically tunable in-line nonlinear saturable absorber, where the laser operation could be tuned from continuous wave, through Q-switched to passively mode-locked regime.

In graphene-side-polished fiber, a high index polyvinyl butyral layer that is put on the graphene film can help to draw out the evanescent tail of the propagating core mode and enhance the light–graphene interaction. Using this method, a commercial grade broadband graphene-based fiber polarizer with low device loss of ≈ 1 dB was proposed and fabricated in 2016.^[205] It was a TE-pass polarizer with broadband working

range of 1425–1600 nm with high extinction ratio of 26–40 dB and an additional value of 13 dB at 2000 nm.

PCFs with designable structures and functions are good candidate for fiber polarizers. In 2018, a graphene/hBN-coated polished-PCF was proposed theoretically which could be switched between TE- and TM-pass working state by tuning graphene E_F .^[206] The total internal reflection type PCF with six-ring air-hole was covered by graphene/hBN films on its side polished area. Increasing the layer number of graphene, the air hole/space ratio, and the polishing depth could promote its performance with the extinction ratio of 66.26 dB mm⁻¹, and the insertion loss of 9.4 dB mm⁻¹, theoretically.

Most of these reported Gr-optical fiber polarizers have similar structures and working principles. Therefore, more and more works^[9,12,87,207] are focused on how to improve device performance, reduce costs, and optimize fabrication processes, such as increasing extinction ratio, expanding operating wavelength range, increasing modulation depth and speed, and reducing insertion loss and absorption loss. Although they have obvious advantages of being compact and tunable, the coupling loss and fabrication difficulties limit their applications in practical all-fiber systems.

The broadband absorption short recovery time, low saturation fluence, high nonlinearity, and high modulation depth of graphene attracts a lot of attention on its pulsed fiber laser applications. These fiber lasers are based on the graphene-fiber end surface, the graphene-side-polished fibers, and the graphene-tapered-fibers. Most of them are passive mode-locked fiber lasers and passive Q-switched fiber lasers with graphene as the saturable absorbers. Actively Q-switched graphene fiber lasers are realized based on all-optical modulation effect of graphene. The transmittance of signal light can be modulated periodically by another laser pulse chain through graphene, which controls the Q-factor of the cavity.

The first pulsed laser based on Gr-optical fiber was realized by Bao et al. in 2009.^[19] Graphene film was transferred on the end face of a fiber connector as saturable absorbers in a fiber laser for generating ultrashort pulses at 1567 nm, with a pulse duration of 756 fs, a repetition rate of 1.79 MHz, and a maximum average output power up to 2 mW. In a similar structure, a passively mode-locked erbium-doped fiber laser with 460 fs pulse duration at 1559 nm was demonstrated in 2010.^[21] Since then, graphene-based saturable absorbers have been used in fiber lasers of various structures to achieve pulse output with different wavelengths, repetition rates, and pulse durations, as well as different principles including passively mode-locked,^[208] passively Q-switched,^[209] and actively Q-switched.^[210]

Gr-optical fibers were used in a high-power fiber lasers reported in 2014, where the system utilized a low-power seed laser mode-locked with graphene saturable absorber emitting soliton pulses at 50 MHz repetition rate.^[211] Then, the seed laser went through the process of temporally stretching, amplifying, and compressing, and finally output 835 fs-short pulses with 8.65 W of average power.

Fiber knot resonators can be used to produce ultrahigh repetition-rate pulse fiber lasers based on the dissipative four-wave mixing mode-locking technique. By virtue of the excellent nonlinear optical response of graphene, Luo et al. proposed

a graphene-decorated microfiber knot as the broadband resonator for generation of the four-wave mixing in 2018.^[212] An ultrahigh-repetition-rate pulses at with 162 and 106.7 GHz were generated at 1.06 and 1.55 μm wavebands, respectively.

Graphene-based passively Q-switched dual-wavelength erbium-doped fiber laser was demonstrated by Cai et al. in 2010, where graphene was transferred on the fiber end surface by optical radiation method in a graphene solution.^[213] The Gr-optical fiber played the key role of the passive Q switcher. The strong optical nonlinearity of graphene was helpful for eliminating the mode competition of erbium-doped fiber for stabilizing the dual wavelength lasing. This Gr-optical fiber laser showed a wide range of pulse-repetition rate from 3.3 to 65.9 kHz, and pulse duration of 3.7 μs around ≈ 1566 nm.

In 2015, an actively Q-switched ytterbium-doped fiber laser was fabricated with a Gr-tapered-optical fiber as the all-optical Q-switcher and ytterbium-doped fiber as the gain medium.^[214] Based on the cross-absorption modulation effect of graphene, a stable Q-switched pulse train of 1060 nm was generated when a 1550 nm pulse laser was incident into the Q-switcher. The narrowest pulse duration was 2.16 μs and its repetition rate could be tuned from 30 to 101 kHz.

In a compact graphene-coated distributed feedback Bragg-grating fiber laser, a single-frequency actively Q-switching was demonstrated and investigated by Wong et al. in 2017, which was with μs pulse durations and sub-MHz spectral linewidths at ≈ 1544 nm.^[209] Part of fiber cladding of distributed feedback Bragg-grating was etched away by using buffered oxide etch, and monolayer graphene was wrapped around the etched section via the wet transfer method. A pump light from a tunable 980 nm laser module was utilized to periodically modulate the optical absorption loss of the graphene at 1544 nm.

Gr-optical fiber pulsed lasers have good tunability, stability, compactness, and robustness, with potential impact in optical coherent communications, metrology, and sensing. Similar to polarizers, all Gr-optical fiber lasers are based on the saturable absorption effect, electro-optic modulation, and all-optical modulation effect of graphene, therefore more and more works would focus on how to improve fiber laser performance with various structure designs.^[87,115,215]

The Gr-optical fibers are also widely studied in the fields of fiber modulators and fiber sensors, which benefits from the various structures of fiber devices including fiber gratings, fiber cavities, and fiber interferometers, and the various good properties of graphene including the surface plasmon effect, all-optical modulation effect, opto-thermal effect, magneto-optic effect, and electro-optic effect. The enhanced light-graphene interaction in Gr-optical fibers contributes to their application greatly as well. Gr-optical fiber sensors not only have the advantages of common optical fiber sensors but also can measure more parameters with higher sensitivity and resolution.

Although Gr-optical fiber devices have been applied to many applications, much work remains to be done before commercial devices can be realized. The transfer methods are still not perfect enough. It is difficult to guarantee that graphene is uniformly distributed and not damaged, wrinkled, or polluted, during the transfer process. In addition, the size and thickness of graphene film couldn't be control well.

4.2. Graphene Photonic Crystal Fiber Devices

In Gr-PCFs, the core-guided light mainly interacts with the graphene films tightly attached to the innermost hole walls through the evanescent wave at the interface of graphene and silica, in which more of the electric field of the fundamental mode is distributed in the graphene layers. Experimentally, a strong attenuation of $\approx 8.3 \text{ dB cm}^{-1}$ is verified, in striking contrast to the value of 0.1 dB in suspended monolayer graphene. This greatly enhanced light–graphene interaction in Gr-PCFs results from the enlarged effective interaction area and length during light propagation along the fiber core (Figure 5a,a1).^[88]

Because Gr-PCFs inherit the electro–optic tunable properties and wide wavelength response of graphene, Gr-PCFs have great potential to be exploited as various all-fiber devices, in which the unprecedented electrical tunability of the light–graphene interaction could not be more appropriate for a modulator, which is one of the key devices in optical fiber communication. However, structural design of the electro–optic modulator based on Gr-PCFs is challenging. Graphene electro–optic modulation devices generally consist of a graphene-insulator-metal sandwich structure on a SiO_2/Si substrate, where SiO_2 of 300 nm thickness acts as an insulating layer, which usually works at a voltage of $\approx 100 \text{ V}$.^[22,216] If the Gr-PCF electro–optic modulator adopts such a sandwich structure of graphene/fiber cladding/metal where the metal is deposited on the outside surface of the fiber cladding, then $\approx 3000 \text{ V}$ is estimated to be required to drive the fiber modulator for the extremely thick SiO_2 cladding of $\approx 100 \mu\text{m}$. Such a high working voltage is obviously inappropriate for a small fiber modulator. In 2019, an ingenious design was developed in which an ionic liquid was injected into the Gr-PCF holes to shift the E_F of graphene, control the light transmittance, and realize an all-fiber graphene fiber electro–optic modulator (Figure 5a). The ionic liquid possesses a large capacitance such that a low gate voltage of only several volts can efficiently dope graphene, during which an electrical double layer with an $\approx 1 \text{ nm}$ thickness is formed at the graphene–ionic liquid interface. As expected, this modulator shows a broadband spectral response from 1150 to 1600 nm, a low operating voltage of $< 2 \text{ V}$, and high modulation depths of ≈ 13 and $\approx 20 \text{ dB cm}^{-1}$ at the fiber-optic communication O-wavelength (1310 nm) and C-wavelength (1550 nm) bands, respectively. Although ionic liquid gating technology solves the problem of a high driving voltage, it also results in the shortcoming of a low switching speed of $\approx 16 \text{ Hz}$ due to the slow response speed (or the large time constant) of the ionic liquid (Figure 5a2).

An ultrahigh response speed of $\approx 500 \text{ GHz}$ for graphene was theoretically confirmed because of the fast relaxation time of excited electrons in graphene (Figure 3a6).^[20,26] Therefore, there is much room to upgrade the slow response speed of the Gr-PCF modulator. A Gr-PCF modulator with a high speed and a large modulation depth was theoretically proposed in 2020, in which graphene/hexagonal boron nitride/graphene (Gr/hBN/Gr) films were directly attached to the fiber hole walls (Figure 5b–b2).^[217] In the sandwich structure, the solid 2D insulator material of hBN as the spacer in the dual graphene FET can realize a negligible delay effect on the modulation time. Therefore, the bandwidth is mainly limited by the response time constant of the equivalent circuit $f = 1/(2\pi RC)$.

On the basis of guaranteeing a broad optical communication wavelength (from the O-band to the U-band), the modulation depth, modulation speed, and driving voltage can be designed when the layer numbers of graphene and hBN and the structure parameters of the fiber length, hole pitch, and diameter are specially designed. In this Gr/hBN/Gr-PCF, the 2D heterostructure with nanometer thickness does not affect the fundamental mode, and the transmitted light is confined in the solid fiber core in the form of a fundamental guiding mode, similar to the bare PCF.

When the PCF has a hole diameter of $\Phi = 1 \mu\text{m}$, a pitch of $\Lambda = 1.516 \mu\text{m}$, and single layer graphene and hBN films, the modulator shows a strongly enhanced light–graphene interaction with a large transmission attenuation coefficient of up to 42.4 dB mm^{-1} at 1550 nm. It can work with single-mode transmission from 1260 to 1700 nm and a high modulation depth from 35 to 50 dB mm^{-1} by shifting E_F (corresponding to a theoretical driving voltage from 28.3 to 15.6 V). Its bandwidth is greatly affected by the fiber length and slightly changed by the carrier concentration of graphene. The modulator with a fiber length from 1 to 0.1 mm can achieve a 1 MHz–0.1 GHz bandwidth regardless of the graphene carrier concentration varying from 1.5×10^{13} to $8.1 \times 10^{11} \text{ cm}^{-2}$. In brief, the proposed Gr-PCF modulator exhibits high electro–optic modulation depth and speed (up to $\approx 0.1 \text{ GHz}$), broad optical communication wavelength (1260–1700 nm), significant modulation depth (e.g., $\approx 42 \text{ dB mm}^{-1}$ at 1550 nm), and relatively low driving voltage (below 30 V). With the development of low-dimensional material manufacturing technology, such Gr/hBN/Gr-PCF is expected to be realized by the CVD method in the future based on reported technologies with which graphene/hBN heterojunctions and Gr-PCFs have both been successfully achieved.^[88,218]

An all-optical modulator based on Gr-PCF is demonstrated in 2020, where Gr-PCF is directly CVD-grown using methane as carbon precursor at $\approx 1030 \text{ }^\circ\text{C}$ under atmospheric pressure.^[219] In the all-optical modulator experiment, 2 cm long Gr-PCF is connected with standard single mode fibers, coupled by two light beams at 1550 and 895 nm simultaneously using a wavelength division multiplexer. The output intensity of 895 nm laser is modulated by the different input intensity of 1550 nm, where the modulation depth increases with the increment of 1550 nm laser power, and achieves the maximum of $\approx 2.58 \text{ dB}$ under 60 mW.

Similar to traditional optical fibers, Gr-PCFs also have good features for sensing. Traditional optical fiber temperature sensors are mainly based on fiber gratings or interferometers, where the optical signals are sensed through the grating pitch variation or optical path difference caused by the disturbed environment temperature. However, these fiber temperature sensors suffer from complicated structural designs and wavelength-resolved measurement systems. To overcome this dilemma, a tunable and highly sensitive temperature sensor based on a Gr-PCF was theoretically proposed in 2021 (Figure 5c–c2).^[220] The mechanism of this hybrid Gr-PCF sensor is directly related to the Fermi–Dirac distribution change of the electrons with temperature, which means variation of the graphene conductivity (including both the real and imaginary parts). When the temperature rises from -100 to $100 \text{ }^\circ\text{C}$, the

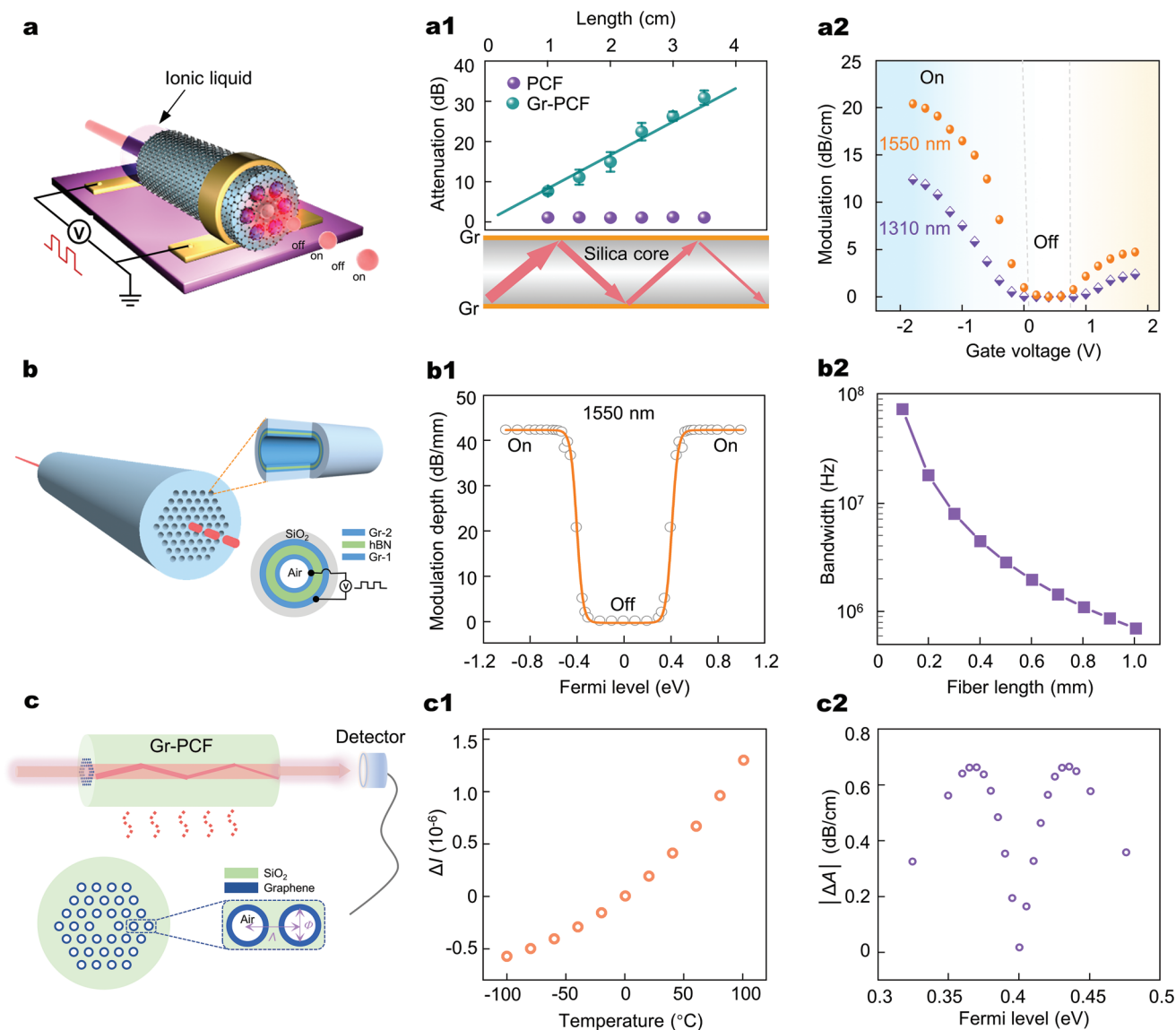


Figure 5. Schematic of Gr-PCF devices. a) Schematic of a Gr-PCF-based electro-optic modulator. The gate voltage between the ionic liquid and graphene controls light transmission through the Gr-PCF. a1) Top: measured optical attenuation of light propagating in the bare PCF (purple dots) and Gr-PCF (cyan dots) with different fiber lengths. The attenuation coefficient is fitted as 8.3 dB cm^{-1} from the slope. Bottom: schematic of attenuation of light with multiple reflections during its propagation along the Gr-PCF core. a2) Modulation curves at 1310 and 1550 nm showing an unambiguous transition between the “on” and “off” states with a large modulation depth. b) Schematic illustration of a sandwiched Gr/hBN/Gr-PCF modulator. b1) Modulation curve of the modulator at 1550 nm. b2) The modulator bandwidth shows an inverse relationship with the fiber length. In this modulator, 100-layer hBN and two monolayer graphene films are attached to the hole surface. c) Schematic of the Gr-PCF temperature sensor, where the Fermi-Dirac distributions of electrons in graphene at different temperatures result in changes in the conductivity and complex refractive index of graphene. c1) Relative normalized intensity (ratio of the intensity at the innermost graphene position to that at the fiber core center) ΔI with temperature from -100 to $100 \text{ }^\circ\text{C}$. Here, Δ represents the difference between the value at a given temperature and that at $0 \text{ }^\circ\text{C}$. c2) $|\Delta A|$ (difference in light attenuation between the temperatures of -100 and $100 \text{ }^\circ\text{C}$) changes with E_F showing a dip value at $E_F = 0.4 \text{ eV}$. a,a1,a2) Reproduced with permission.^[88] Copyright 2019, Nature Publishing Group. b,b1,b2) Reproduced with permission.^[217] Copyright 2020, Royal Society of Chemistry. c,c1,c2) Reproduced with permission.^[220] Copyright 2021, IOP Publishing.

imaginary part decreases, followed by a decrease in graphene absorption; at the same time, the real part increases along with the increase in the refractive index in the fiber cladding, which leads to the consequent enhancement of the normalized light intensity. Taking the influences of both the imaginary and real parts into account, the change in the transmission attenuation of the Gr-PCF is $6.4 \times 10^{-5} \text{ dB cm}^{-1}$. In addition, this all-fiber

temperature sensor theoretically exhibits a tunable sensitivity by modulating the graphene E_F , with the highest sensitivity of up to $\approx 3.34 \times 10^{-3} \text{ dB cm}^{-1} \text{ }^\circ\text{C}^{-1}$ at $E_F = 0.435 \text{ eV}$ when it is set to work at a laser wavelength of 1550 nm (Figure 5c2). Furthermore, by optimizing the PCF hole diameter to $1 \mu\text{m}$ and subsequently enhancing the light-graphene interaction, its sensitivity can be improved by approximately ten times to

0.036 dB cm⁻¹ °C⁻¹. The work provides highly sensitive temperature sensors based on a Gr-PCF and broadens the applications of all-fiber optoelectronic devices.

The all-fiber devices based on Gr-PCFs have easy electro-optic tunability and broad spectral response characteristics, which have important potential application value. Realization of more all-optical devices based on Gr-PCFs with the advancement of growth technology and device processing technology is expected.

4.3. The Related 2D Material-Photonic Crystal Fiber Devices

The 2D material-PCFs, in which 2D materials are grown on PCF hole walls, have many performance advantages, but the technical difficulty of the fabrication is obviously higher than that of wrapping them on the surface of tapered or side-polished fibers. Therefore, to date, only a few related works have been reported on other 2D material-PCFs, such as MoS₂-PCFs (and other transition metal dichalcogenides, TMDs).

The other 2D materials-traditional fibers by CVD method are rarely reported. The reason is likely that transfer method is less difficult than CVD method for fiber device applications. In 2019, Gu et al. for the first time grew single-crystal monolayer MoS₂ on tapered silica optical fibers, and then they used a simple photoactivation strategy to obtain strongly enhanced and highly stable photoluminescence quantum yields in a wide pump dynamic range at room temperature.^[221] The ≈3 cm optical fiber was suspended and fixed on two motor-driven stages. And taper structures or microbottle structures were fabricated by CO₂ laser heating. The taper-drawing process greatly lowered the activation energy from siloxane bonds in bulky amorphous silica. The highly strained siloxane bonds could be easily excited to release high-density oxygen dangling bonds on the fiber surface under high intensity light irradiation of 532 nm laser, which was the key to achieving strong photoluminescence enhancement. The photoluminescence quantum yields of as-photoactivated MoS₂ monolayer on tapered-fiber of ≈3 μm in diameter was enhanced by two orders of magnitude (from ≈30% to 1% as pump intensity increases from 10⁻¹ to 10⁴ W cm⁻²), compared with the planar monolayer samples grown on silica substrates (quantum yields of <0.05%). Based on the above conclusions, they made microbottle structures of optical fiber as good optical microcavities, and used the 532 nm continuous-wave laser to excite an as-activated monolayer MoS₂ on microfiber to realize a continuous-wave whispering-gallery mode lasing action with low-threshold at room temperature. Their strategy provides an exciting direction for efficient and stable light sources with low-threshold at room temperature based on these atomically thin materials.

Direct CVD growth of MoS₂-PCFs was demonstrated for the first time in 2020,^[175] which showed extremely enhanced second-harmonic generation (SHG) and third-harmonic generation (THG) and was further exploited to realize an all-fiber mode-locked laser with a MoS₂-PCF as a saturable absorber (Figure 6).

Unlike the gas feedstocks used in the CVD growth of Gr-PCFs, the CVD growth of TMDs, including MoS₂, generally requires solid feedstock precursors, which are very difficult

to transfer into fiber holes effectively and homogeneously. An ingenious two-step CVD method has been employed that alleviates this dilemma, in which a solid precursor is predeposited via capillarity and drying of a Na₂MoO₄ aqueous solution to guarantee a homogeneous feedstock along the entire PCF holes. Finally, large and uniform monolayer MoS₂ films with high quality are grown on the hole walls of hollow capillary fibers and HCFs. Following a similar method, other 2D TMDs of WS₂, MoSe₂, and MoS_xSe_{2-x} alloys have been obtained by varying the feedstocks of the transition metal (e.g., Na₂MoO₄ and Na₂WO₄) and chalcogen (e.g., S and Se) species with adjusted growth temperatures.

Due to the strongly enhanced light-matter interaction and the ultrahigh optical nonlinearity of 2D MoS₂ in MoS₂-PCFs, the authors applied these properties to nonlinear wavelength conversion and an ultrafast fiber laser. Under 1800 and 2100 nm laser excitation in monolayer MoS₂-based hollow capillary fibers with a length of up to ≈25 cm, both the SHG and THG can be enhanced by ≈300 times compared to that obtainable with monolayer MoS₂ on a flat, fused silica substrate (Figure 6a–a2). The MoS₂-HCF with six to eight layer-MoS₂ and a 3 cm length shows a nonlinear absorption modulation depth of 10% with a saturation peak intensity of 0.8 MW cm⁻² at 1550 nm, whose values are already comparable to those of conventional saturable absorber semiconductors (e.g., a modulation depth of ≈5% with a saturation peak intensity of ≈2 MW cm⁻² for AlAs/GaAs Bragg mirrors). A stretched-pulse passively mode-locked fiber laser was built based on the MoS₂-PCF, which output a pulse train with an ≈500 fs pulse duration, an ≈41 MHz repetition frequency, a 1560 nm center wavelength, and a maximum output power of ≈6 mW. This work opens up a new regime for the design of nonlinear optical materials and demonstrates the practical application of 2D material-PCFs (Figure 6b–b2).

A novel electro-optic modulator based on MoS₂-PCFs was reported in 2020 via external electrical gating of 2D MoS₂ bilayers deposited within the inner regions of a silica hollow-core antiresonant PCF with an eight-ring tubular structure.^[222] Liquid phase deposition techniques were used, in which the single-source precursor of ammonium tetrathiomolybdate mixed into a solvent solution penetrated into the hole regions of the fiber through capillary action. After the annealing process at 500 °C in a horizontal furnace, MoS₂-PCFs were obtained with an almost constant bilayer film along the 40 cm length of the fiber. The MoS₂-PCF was placed on a metallic slab with a varying DC voltage of up to 1500 V and consequently showed an intensity change of the output spectrum as the applied voltage changed from 0 to 1500 V. This is because the fundamental mode with power focused into the center of the fiber at the voltage of 0 V turns into a disordered mode with a reduced output power at high voltages. That is, electro-optic modulation of the modal properties of the transmission is implied. The output shows a large intensity drop of 3.52 dB at a wavelength of 744.2 nm.

In 2020, Eilenberger et al. directly CVD-grew monolayer MoS₂ and WS₂ on the core of all-silica microstructured exposed-core PCFs (Figure 6c).^[223] The suspended core PCF where the core of 2 μm in diameter was suspended by three struts to the fiber cladding of 220 μm in diameter, had been cut open on one side to expose one part of the central section of the fiber since it was an ultrasonic-drilled silica preform. A modified CVD growth

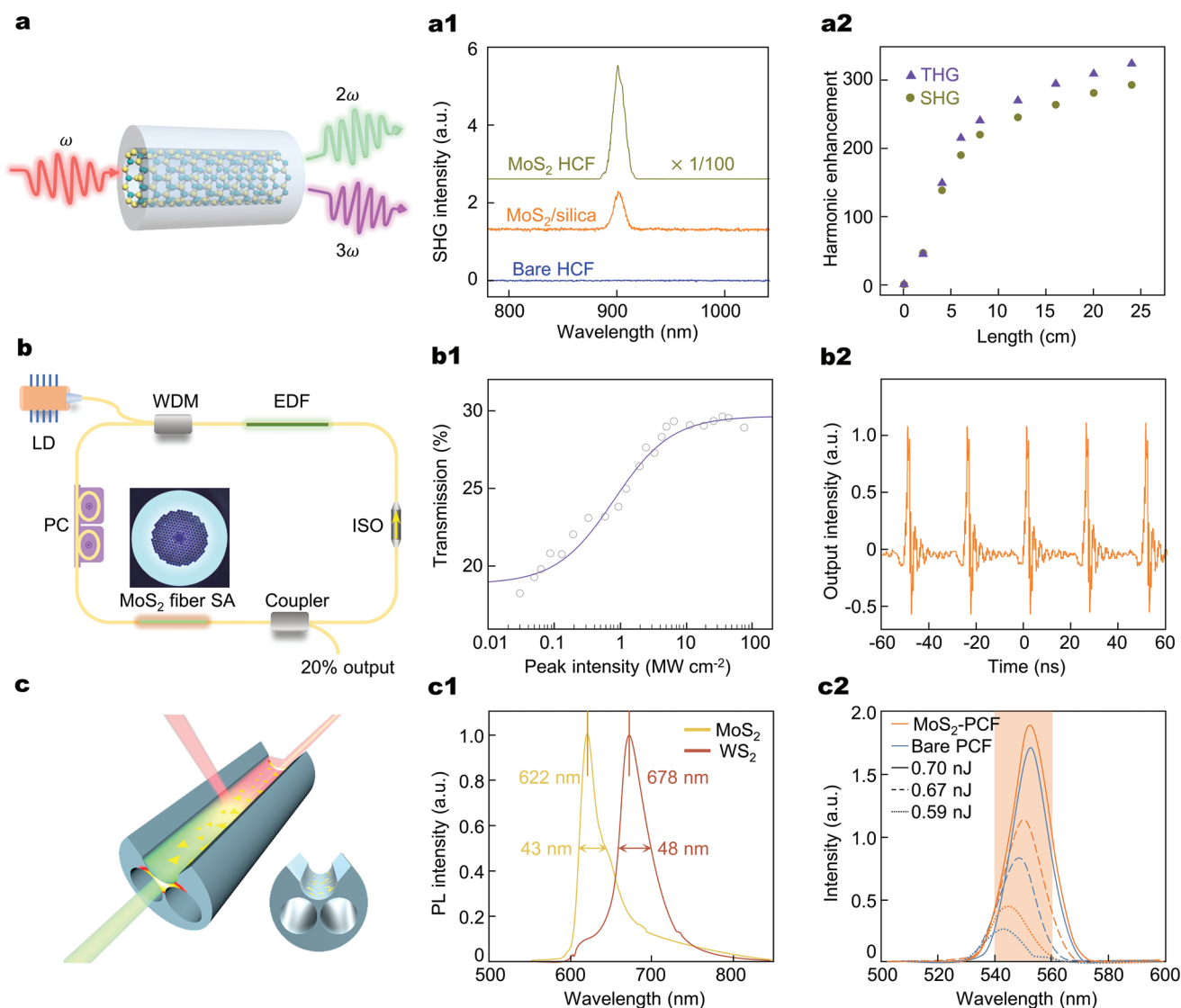


Figure 6. Schematic of MoS₂-PCFs application. a) Greatly enhanced SHG and THG in a MoS₂-embedded hollow capillary fiber with a diameter of $\approx 5 \mu\text{m}$. a1) SHG spectra of a MoS₂-HCF, MoS₂ on a flat, fused silica substrate (MoS₂/silica), and a bare HCF under 1800 and 2100 nm excitation (note: HCF is a hollow capillary fiber here). With the strong light–matter interaction in the 25-cm-long MoS₂-HCF, both SHG and THG can be enhanced by ≈ 300 times compared with monolayer MoS₂/silica. a2) Fiber-length-dependent-SHG and -THG enhancements in the MoS₂-HCF with respect to MoS₂/silica, showing a general monotonic increase and saturation behavior with the fiber length. b) Schematic of an all-fiber mode-locked laser with a MoS₂-embedded HCF (insert picture) as a saturable absorber (SA). b1) Transmission measurement of the MoS₂-PCF for 10% of the nonlinear absorption modulation depth. The solid curve is fitted according to the experimental data (circles). b2) Output ultrafast pulse train with an ≈ 24 ns interval (i.e., an ≈ 41 MHz repetition rate) and a pulse duration of ≈ 500 fs. c) A PL experiment of the CVD-grown monolayer MoS₂ or WS₂ crystals on the core of exposed-core PCF. c1) Normalized PL spectra of MoS₂- and WS₂-PCFs excited by a 532 nm laser. c2) Third-harmonic spectra of MoS₂-PCF. The spectral band from 540 to 560 nm is marked in orange. a, a1, a2, b, b1, b2) Reproduced with permission.^[175] Copyright 2020, Nature Publishing Group. c, c1, c2) Reproduced with permission.^[223] Copyright 2020, Wiley-VCH.

method with a Knudsen-type effusion cell for the chalcogen precursors was used to grow MoS₂ and WS₂ film on the entire outer surface of fiber and on the exposed upper surface of the core. A green laser at 532 nm was coupled into the MoS₂- or WS₂-PCF which excited excitons of MoS₂ or WS₂ via the evanescent field of the fundamental modes. The exciton fluorescence at 678 nm (MoS₂) and 622 nm (WS₂) was either emitted into free space or coupled back into the fiber mode (Figure 6c1). When a pulse laser at $\lambda_0 = 1570$ nm with a pulse duration of 32 fs was coupled into the MoS₂-PCF, the enhanced THG signals were

in a spectral band ranging from 540 to 560 nm rather than at exact $\lambda_0/3 \approx 523$ nm (Figure 6c2). The reason was that the fundamental wave spectrum nonlinearly broadened into a THG relevant sub-band between 1620 to 1680 nm before THG was generated. Besides, the addition of the MoS₂ or WS₂ coating didn't enhance the nonlinear interaction for all higher-order THG modes equally but it just boosted those that were localized close to the surface and with predominant x-polarization. Their works may open a novel route to remote sensing and yield a new avenue to tailor nonlinear optical processes in fibers.

5. Perspectives and Conclusions

In this paper, we have performed a comprehensive review of Gr-PCFs. The review primarily covers the introduction of graphene and PCFs with many distinctive characteristics and the development of Gr-PCF growth methods and Gr-PCF-based devices. From an overall perspective, a Gr-PCF can be considered a new hybrid fiber with the many excellent properties and superiorities inherited from both graphene and PCFs, which also provides a new development direction and abundant opportunities for graphene and optical fibers.

Gr-PCFs perfectly combine the structural properties of PCFs and the material properties of graphene, which greatly intrigues scientists, and provides obvious and unique advantages of keeping the PCF structure and main optical functions intact, the strongly enhanced and tunable light–graphene interaction, the rich designable structures with versatility, and the easy mass-production by CVD.

Note that Gr-PCFs as well as Gr-traditional fibers remain at proof-of-concept or prototype stages, and many key challenges are still waiting to be addressed toward the ultimate practical applications. Future development of Gr-optical fibers may be divided into three directions: growth technology, design and application of fiber devices, and system integration of different fiber devices where most devices are based on graphene optical fibers with different structures and functions of signal emitting, transmission, modulation, and detection. This will inevitably encounter a lot of difficult challenges, but also accompanied by opportunities.

The CVD growth method to produce graphene or other 2D materials in PCF may provide the ultimate solution to most of the hybrid fiber devices, because the conventional mechanical transfer of 2D materials to fiber structures are time consuming and not scalable, and the unintentional doping and structural defects are easily introduced to hybrid fiber devices, which will significantly influence their optoelectronic performance. This requires that large-area single-crystal graphene or graphene heterojunctions with uniform layer thickness can be grown in fiber holes of different shapes and sizes. And heterojunctions consisting of graphene and other 2D materials are likely to be CVD-grown in PCFs to form new hybrid fibers. However, the kinetic process of the growth of graphene and other 2D materials in PCF holes with micrometer-diameter is not fully understood. For example, graphene growth is almost impossible to achieve in air hole smaller than 2 μm in diameter. The fiber becomes more brittle due to the hydrogen used to assist graphene growth during the preparation of the graphene fiber, as well as the high temperature and cooling process. This change brings great difficulties to the fusion and reprocessing of fiber and fiber device. The way to solve this problem is to use high temperature resistant silica fiber, improve the fiber preparation process, or reduce the growth temperature of graphene fiber, but obviously these methods are full of challenges. In addition, the accurate characterization still needs to remove the optical fiber by etching, but this is time consuming and sacrifices the integrity of its overall structure. Therefore, there is another pressing issue on how to characterize the thickness accurately and efficiently, defects, crystal domain sizes, defects, and other physical properties of graphene films on the PCF hole walls, which is hindered by a thick quartz fiber cladding.

As for the future development of hybrid fiber devices, the novel materials and advanced PCF structures are two important ingredients for photonic and optoelectronic integration. Graphene can be combined with hBN, TMDs (MX_2 , $\text{M} = \text{Mo}, \text{W}$; $\text{X} = \text{S}, \text{Se}, \text{Te}$), and other 2D materials to form a heterojunction with unusual physics and properties.^[224,225] For example, TMDs with exotic optical and electronic properties are combined with graphene with wide spectral response range, which could extend the optical spectra of photodetection and light emitting in fibers. Based on the high nonlinearity of graphene and hBN, hybrid optical fibers based on graphene-hBN heterostructure could be applied to generate supercontinuum white light, wavelength conversion, high-harmonic generation, nonlinear parametric amplification, optical soliton generation, and other optical effects. Similar to graphene-tapered fibers and side-polished fibers, Gr-PCFs could also be used for pulsed fiber laser, which has the advantage that graphene is isolated from the external environment by the PCF. The advanced PCF structures could bring more opportunities for high-performance fiber optic devices, such as two-arm Mach–Zehnder interferometer, fiber knot ring resonator, fiber grating, twisted coreless PCF, twin-core PCF, and double clad PCF, which would be used for all-optical phase shifter and switch, optical frequency combs, interferometers, modulators, sensors, or others.

Similar to the hybrid PCFs filled with gases, liquids, and solids, graphene PCFs and 2D material-PCFs have their own unique advantages for application in various fields. Although Gr-PCFs are still in their infancy and still confined to the theory and laboratory studies, the future for Gr-PCFs and similar 2D materials-PCFs look very exciting and have great scientific research and application values, from the point of view of the development history and potential of graphene and optical fibers. In order to achieve the ideal result, the preparation methods, the structures, and devices of Gr-PCFs, need to be constantly improved. It is hoped that this review can play a role in attracting more attention to the preparation and application of Gr-PCFs, and promote the development of Gr-PCFs.

Acknowledgements

The authors gratefully acknowledge the support from National Natural Science Foundation of China (52102044, T2188101, and 92163206), Beijing Science and Technology Project (Z181100004818003), and the National Key R&D Program of China (2021YFA1400502).

Conflict of Interest

The authors declare no conflict of interest.

Keywords

chemical vapor deposition, fiber devices, graphene, optical fibers, photonic crystal fibers

Received: February 26, 2022
Revised: April 10, 2022
Published online:

- [1] K. S. Novoselov, A. K. Geim, S. V. Morozov, D. Jiang, Y. Zhang, S. V. Dubonos, I. V. Grigorieva, A. A. Firsov, *Science* **2004**, 306, 666.
- [2] K. S. Novoselov, D. Jiang, F. Schedin, T. J. Booth, V. V. Khotkevich, S. V. Morozov, A. K. Geim, *Proc. Natl. Acad. Sci. USA* **2005**, 102, 10451.
- [3] A. K. Geim, K. S. Novoselov, *Nat. Mater.* **2007**, 6, 183.
- [4] K. S. Novoselov, V. I. Fal'ko, L. Colombo, P. R. Gellert, M. G. Schwab, K. Kim, *Nature* **2012**, 490, 192.
- [5] M. Romagnoli, V. Sorianello, M. Midrio, F. H. L. Koppens, C. Huyghebaert, D. Neumaier, P. Galli, W. Templ, A. D'Errico, A. C. Ferrari, *Nat. Rev. Mater.* **2018**, 3, 392.
- [6] R. R. Nair, P. Blake, A. N. Grigorenko, K. S. Novoselov, T. J. Booth, T. Stauber, N. M. R. Peres, A. K. Geim, *Science* **2008**, 320, 1308.
- [7] A. H. C. Neto, F. Guinea, N. M. R. Peres, K. S. Novoselov, A. K. Geim, *Rev. Mod. Phys.* **2009**, 81, 109.
- [8] A. A. Balandin, *Nat. Mater.* **2011**, 10, 569.
- [9] Q. L. Bao, K. P. Loh, *ACS Nano* **2012**, 6, 3677.
- [10] A. N. Grigorenko, M. Polini, K. S. Novoselov, *Nat. Photonics* **2012**, 6, 749.
- [11] X. Huang, Z. Y. Zeng, Z. X. Fan, J. Q. Liu, H. Zhang, *Adv. Mater.* **2012**, 24, 5979.
- [12] N. O. Weiss, H. L. Zhou, L. Liao, Y. Liu, S. Jiang, Y. Huang, X. F. Duan, *Adv. Mater.* **2012**, 24, 5782.
- [13] G. Fiori, F. Bonaccorso, G. Iannaccone, T. Palacios, D. Neumaier, A. Seabaugh, S. K. Banerjee, L. Colombo, *Nat. Nanotechnol.* **2014**, 9, 768.
- [14] W. Han, R. K. Kawakami, M. Gmitra, J. Fabian, *Nat. Nanotechnol.* **2014**, 9, 794.
- [15] M. F. El-Kady, Y. Shao, R. B. Kaner, *Nat. Rev. Mater.* **2016**, 1, 16033.
- [16] C. Wang, K. Xia, H. Wang, X. Liang, Z. Yin, Y. Zhang, *Adv. Mater.* **2019**, 31, 1801072.
- [17] K. Kim, J. Y. Choi, T. Kim, S. H. Cho, H. J. Chung, *Nature* **2011**, 479, 338.
- [18] F. Bonaccorso, Z. Sun, T. Hasan, A. C. Ferrari, *Nat. Photonics* **2010**, 4, 611.
- [19] Q. L. Bao, H. Zhang, Y. Wang, Z. H. Ni, Y. L. Yan, Z. X. Shen, K. P. Loh, D. Y. Tang, *Adv. Funct. Mater.* **2009**, 19, 3077.
- [20] P. A. George, J. Strait, J. Dawlaty, S. Shivaraman, M. Chandrashekar, F. Rana, M. G. Spencer, *Nano Lett.* **2008**, 8, 4248.
- [21] Z. P. Sun, T. Hasan, F. Torrisi, D. Popa, G. Privitera, F. Q. Wang, F. Bonaccorso, D. M. Basko, A. C. Ferrari, *ACS Nano* **2010**, 4, 803.
- [22] F. Schwierz, *Nat. Nanotechnol.* **2010**, 5, 487.
- [23] T. Mueller, F. Xia, *Nat. Photonics* **2010**, 4, 297.
- [24] X. T. Gan, R. J. Shiue, Y. D. Gao, I. Meric, T. F. Heinz, K. Shepard, J. Hone, S. Assefa, D. Englund, *Nat. Photonics* **2013**, 7, 883.
- [25] A. Pospischil, M. Humer, M. M. Furchi, D. Bachmann, R. Guider, T. Fromherz, T. Mueller, *Nat. Photonics* **2013**, 7, 892.
- [26] M. Liu, X. B. Yin, E. Ulin-Avila, B. S. Geng, T. Zentgraf, L. Ju, F. Wang, X. Zhang, *Nature* **2011**, 474, 64.
- [27] C. T. Phare, Y.-H. D. Lee, J. Cardenas, M. Lipson, *Nat. Photonics* **2015**, 9, 511.
- [28] H. Lin, Y. Song, Y. Huang, D. Kita, S. Deckoff-Jones, K. Wang, L. Li, J. Li, H. Zheng, Z. Luo, H. Wang, S. Novak, A. Yadav, C.-C. Huang, R.-J. Shiue, D. Englund, T. Gu, D. Hewak, K. Richardson, J. Kong, J. Hu, *Nat. Photonics* **2017**, 11, 798.
- [29] B. Yao, Y. Liu, S.-W. Huang, C. Choi, Z. Xie, J. F. Flores, Y. Wu, M. Yu, D.-L. Kwong, Y. Huang, Y. Rao, X. Duan, C. W. Wong, *Nat. Photonics* **2018**, 12, 22.
- [30] V. Bianchi, T. Carey, L. Viti, L. Li, E. H. Linfield, A. G. Davies, A. Tredicucci, D. Yoon, P. G. Karagiannidis, L. Lombardi, F. Tomarchio, A. C. Ferrari, F. Torrisi, M. S. Vitiello, *Nat. Commun.* **2017**, 8, 15763.
- [31] V. Sorianello, M. Midrio, G. Contestabile, I. Asselberghs, J. Van Campenhout, C. Huyghebaert, I. Goykhman, A. K. Ott, A. C. Ferrari, M. Romagnoli, *Nat. Photonics* **2018**, 12, 40.
- [32] B. Yao, S.-W. Huang, Y. Liu, A. K. Vinod, C. Choi, M. Hoff, Y. Li, M. Yu, Z. Feng, D.-L. Kwong, Y. Huang, Y. Rao, X. Duan, C. W. Wong, *Nature* **2018**, 558, 410.
- [33] T. Jiang, D. Huang, J. Cheng, X. Fan, Z. Zhang, Y. Shan, Y. Yi, Y. Dai, L. Shi, K. Liu, C. Zeng, J. Zi, J. E. Sipe, Y.-R. Shen, W.-T. Liu, S. Wu, *Nat. Photonics* **2018**, 12, 430.
- [34] T. Wu, X. Zhang, Q. Yuan, J. Xue, G. Lu, Z. Liu, H. Wang, H. Wang, F. Ding, Q. Yu, X. Xie, M. Jiang, *Nat. Mater.* **2016**, 15, 43.
- [35] X. Z. Xu, Z. H. Zhang, L. Qiu, J. N. Zhuang, L. Zhang, H. Wang, C. N. Liao, H. D. Song, R. X. Qiao, P. Gao, Z. H. Hu, L. Liao, Z. M. Liao, D. P. Yu, E. G. Wang, F. Ding, H. L. Peng, K. H. Liu, *Nat. Nanotechnol.* **2016**, 11, 930.
- [36] Z. Zhang, X. Xu, L. Qiu, S. Wang, T. Wu, F. Ding, H. Peng, K. Liu, *Adv. Sci.* **2017**, 4, 1700087.
- [37] X. Xu, Z. Zhang, J. Dong, D. Yi, J. Niu, M. Wu, L. Lin, R. Yin, M. Li, J. Zhou, S. Wang, J. Sun, X. Duan, P. Gao, Y. Jiang, X. Wu, H. Peng, R. S. Ruoff, Z. Liu, D. Yu, E. Wang, F. Ding, K. Liu, *Sci. Bull.* **2017**, 62, 1074.
- [38] B. Den, Z. W. Xin, R. W. Xue, S. S. Zhang, X. Z. Xu, J. Gao, J. L. Tang, Y. Qi, Y. N. Wang, Y. Zhao, L. Z. Sun, H. H. Wang, K. H. Liu, M. H. Rummeli, L. T. Weng, Z. T. Luo, L. M. Tong, X. Y. Zhang, C. S. Xie, Z. F. Liu, H. L. Peng, *Sci. Bull.* **2019**, 64, 659.
- [39] L. Lin, H. L. Peng, Z. F. Liu, *Nat. Mater.* **2019**, 18, 520.
- [40] L. Lin, J. Zhang, H. Su, J. Li, L. Sun, Z. Wang, F. Xu, C. Liu, S. Lopatin, Y. Zhu, K. Jia, S. Chen, D. Rui, J. Sun, R. Xue, P. Gao, N. Kang, Y. Han, H. Q. Xu, Y. Cao, K. S. Novoselov, Z. Tian, B. Ren, H. Peng, Z. Liu, *Nat. Commun.* **2019**, 10, 1912.
- [41] B. Deng, Z. Liu, H. Peng, *Adv. Mater.* **2019**, 31, 1800996.
- [42] J. C. Zhang, L. Z. Sun, K. C. Jia, X. T. Liu, T. Cheng, H. L. Peng, L. Lin, Z. F. Liu, *ACS Nano* **2020**, 14, 10796.
- [43] M. Wu, Z. Zhang, X. Xu, Z. Zhang, Y. Duan, J. Dong, R. Qiao, S. You, L. Wang, J. Qi, D. Zou, N. Shang, Y. Yang, H. Li, L. Zhu, J. Sun, H. Yu, P. Gao, X. Bai, Y. Jiang, Z.-J. Wang, F. Ding, D. Yu, E. Wang, K. Liu, *Nature* **2020**, 581, 406.
- [44] J. Zhang, L. Lin, K. Jia, L. Sun, H. Peng, Z. Liu, *Adv. Mater.* **2020**, 32, 1903266.
- [45] Y. L. Z. Li, L. Z. Sun, H. Y. Liu, Y. C. Wang, Z. F. Liu, *Inorg. Chem. Front.* **2021**, 8, 182.
- [46] B. Jiang, S. Wang, J. Sun, Z. Liu, *Small* **2021**, 17, 2008017.
- [47] X. Z. Xu, R. X. Qiao, Z. H. Liang, Z. H. Zhang, R. Wang, F. K. Zeng, G. L. Cui, X. W. Zhang, D. X. Zou, Y. Guo, C. Liu, Y. Fu, X. Zhou, M. H. Wu, Z. J. Wang, Y. Zhao, E. K. Wang, Z. L. Tang, D. P. Yu, K. H. Liu, *Nano Res.* **2022**, 15, 919.
- [48] K. C. Kao, G. A. Hockham, *Proc. Inst. Electr. Eng.* **1966**, 113, 1151.
- [49] J. C. Knight, T. A. Birks, P. St J. Russell, D. M. Atkin, *Opt. Lett.* **1996**, 21, 1547.
- [50] J. C. Knight, T. A. Birks, R. F. Cregan, P. S. Russell, J. P. de Sandro, *Electron. Lett.* **1998**, 34, 1347.
- [51] J. C. Knight, J. Broeng, T. A. Birks, P. St J. Russell, *Science* **1998**, 282, 1476.
- [52] R. F. Cregan, B. J. Mangan, J. C. Knight, T. A. Birks, P. St J. Russell, P. J. Roberts, D. C. Allan, *Science* **1999**, 285, 1537.
- [53] J. C. Knight, *Nature* **2003**, 424, 847.
- [54] P. Russell, *Science* **2003**, 299, 358.
- [55] W. Jin, J. Ju, H. L. Ho, Y. L. Hoo, A. Zhang, *Front. Optoelectron.* **2013**, 6, 3.
- [56] M. Komanec, D. Dousek, D. Suslov, S. Zvanovec, *Radioengineering* **2020**, 29, 417.
- [57] T. A. Birks, J. C. Knight, P. S. Russell, *Opt. Lett.* **1997**, 22, 961.
- [58] B. T. Kuhlmeier, R. C. McPhedran, C. M. de Sterke, *Opt. Lett.* **2002**, 27, 1684.
- [59] B. T. Kuhlmeier, R. C. McPhedran, C. M. de Sterke, P. A. Robinson, G. Renversez, D. Maystre, *Opt. Express* **2002**, 10, 1285.
- [60] N. A. Mortensen, J. R. Folkner, M. D. Nielsen, K. P. Hansen, *Opt. Lett.* **2003**, 28, 1879.

- [61] J. C. Knight, J. Arriaga, T. A. Birks, A. Ortigosa-Blanch, W. J. Wadsworth, P. S. Russell, *IEEE Photonics Technol. Lett.* **2000**, 12, 807.
- [62] A. Ferrando, E. Silvestre, J. J. Miret, P. Andres, *Opt. Lett.* **2000**, 25, 790.
- [63] A. Cucinotta, S. Selleri, L. Vincetti, M. Zoboli, *J. Lightwave Technol.* **2002**, 20, 1433.
- [64] W. H. Reeves, J. C. Knight, P. S. J. Russell, P. J. Roberts, *Opt. Express* **2002**, 10, 609.
- [65] A. Ortigosa-Blanch, J. C. Knight, W. J. Wadsworth, J. Arriaga, B. J. Mangan, T. A. Birks, P. S. J. Russell, *Opt. Lett.* **2000**, 25, 1325.
- [66] L. An, Z. Zheng, Z. Li, T. Zhou, J. T. Cheng, *J. Lightwave Technol.* **2009**, 27, 3175.
- [67] N. G. R. Broderick, T. M. Monro, P. J. Bennett, D. J. Richardson, *Opt. Lett.* **1999**, 24, 1395.
- [68] N. A. Mortensen, *Opt. Express* **2002**, 10, 341.
- [69] J. Laegsgaard, N. A. Mortensen, J. Riishede, A. Bjarklev, *J. Opt. Soc. Am. B* **2003**, 20, 2046.
- [70] J. Nilsson, D. N. Payne, *Science* **2011**, 332, 921.
- [71] C. Zhang, Y.-y. Zhang, M.-l. Hu, S.-j. Wang, Y.-j. Song, L. Chai, C.-y. Wang, *Opt. Commun.* **2012**, 285, 2715.
- [72] K. Nagayama, M. Kakui, M. Matsui, T. Saitoh, Y. Chigusa, *Electron. Lett.* **2002**, 38, 1168.
- [73] F. Benabid, J. C. Knight, G. Antonopoulos, P. S. J. Russell, *Science* **2002**, 298, 399.
- [74] P. J. Roberts, F. Couny, H. Sabert, B. J. Mangan, D. P. Williams, L. Farr, M. W. Mason, A. Tomlinson, T. A. Birks, J. C. Knight, P. S. J. Russell, *Opt. Express* **2005**, 13, 236.
- [75] W. Belardi, J. C. Knight, *Opt. Lett.* **2014**, 39, 1853.
- [76] B. Debord, A. Amsanpally, M. Chafer, A. Baz, M. Maurel, J. M. Blondy, E. Hugonnot, F. Scol, L. Vincetti, F. Gerome, F. Benabid, *Optica* **2017**, 4, 209.
- [77] S.-f. Gao, Y.-y. Wang, W. Ding, D.-l. Jiang, S. Gu, X. Zhang, P. Wang, *Nat. Commun.* **2018**, 9, 2828.
- [78] W. J. Wadsworth, A. Ortigosa-Blanch, J. C. Knight, T. A. Birks, T. P. M. Man, P. S. Russell, *J. Opt. Soc. Am. B* **2002**, 19, 2148.
- [79] Y. Ni, L. Zhang, L. An, J. D. Peng, C. C. Fan, *IEEE Photonics Technol. Lett.* **2004**, 16, 1516.
- [80] J. C. Knight, D. V. Skryabin, *Opt. Express* **2007**, 15, 15365.
- [81] X. T. Zhao, G. Y. Zhou, S. G. Li, Z. L. Liu, D. B. Wei, Z. Y. Hou, L. T. Hou, *Appl. Opt.* **2008**, 47, 5190.
- [82] R. Buczynski, H. T. Bookey, D. Pysz, R. Stepien, I. Kujawa, J. E. McCarthy, A. J. Waddie, A. K. Kar, M. R. Taghizadeh, *Laser Phys. Lett.* **2010**, 7, 666.
- [83] M. S. Habib, M. S. Habib, S. M. A. Razzak, M. A. Hossain, *Opt. Fiber Technol.* **2013**, 19, 461.
- [84] F. Belli, A. Abdolvand, W. Chang, J. C. Travers, P. S. Russell, *Optica* **2015**, 2, 292.
- [85] H. Xu, Q. Kong, C. Zhou, *Opt. Fiber Technol.* **2021**, 63, 102485.
- [86] T. Tan, X. Jiang, C. Wang, B. Yao, H. Zhang, *Adv. Sci.* **2020**, 7, 2000058.
- [87] J.-h. Chen, Y.-f. Xiong, F. Xu, Y.-q. Lu, *Light: Sci. Appl.* **2021**, 10, 78.
- [88] K. Chen, X. Zhou, X. Cheng, R. Qiao, Y. Cheng, C. Liu, Y. Xie, W. Yu, F. Yao, Z. Sun, F. Wang, K. Liu, Z. Liu, *Nat. Photonics* **2019**, 13, 754.
- [89] C. Lee, X. D. Wei, J. W. Kysar, J. Hone, *Science* **2008**, 321, 385.
- [90] K. Cao, S. Feng, Y. Han, L. Gao, T. H. Ly, Z. Xu, Y. Lu, *Nat. Commun.* **2020**, 11, 284.
- [91] R. A. Suleimanov, N. A. Abdullaev, *Carbon* **1993**, 31, 1011.
- [92] D. Yoon, Y. W. Son, H. Cheong, *Nano Lett.* **2011**, 11, 3227.
- [93] K. V. Zakharченко, A. Fasolino, J. H. Los, M. I. Katsnelson, *J. Phys.: Condens. Matter* **2011**, 23, 202202.
- [94] J. H. Los, K. V. Zakharченко, M. I. Katsnelson, A. Fasolino, *Phys. Rev. B* **2015**, 91, 045415.
- [95] L. A. Openov, A. I. Podlivaev, *Phys. Solid State* **2016**, 58, 847.
- [96] S. R. Wang, Y. Zhang, N. Abidi, L. Cabrales, *Langmuir* **2009**, 25, 11078.
- [97] P. R. Wallace, *Phys. Rev.* **1947**, 71, 622.
- [98] J. C. Slonczewski, P. R. Weiss, *Phys. Rev.* **1958**, 109, 272.
- [99] G. W. Semenoff, *Phys. Rev. Lett.* **1984**, 53, 2449.
- [100] F. D. M. Haldane, *Phys. Rev. Lett.* **1988**, 61, 2015.
- [101] K. S. Novoselov, A. K. Geim, S. V. Morozov, D. Jiang, M. I. Katsnelson, I. V. Grigorieva, S. V. Dubonos, A. A. Firsov, *Nature* **2005**, 438, 197.
- [102] E. V. Castro, H. Ochoa, M. I. Katsnelson, R. V. Gorbachev, D. C. Elias, K. S. Novoselov, A. K. Geim, F. Guinea, *Phys. Rev. Lett.* **2010**, 105, 266601.
- [103] N. Tombros, A. Veligura, J. Junesch, J. J. van den Berg, P. J. Zomer, M. Wojtaszek, I. J. V. Marun, H. T. Jonkman, B. J. v. Wees, *J. Appl. Phys.* **2011**, 109, 093702.
- [104] S. V. Morozov, K. S. Novoselov, M. I. Katsnelson, F. Schedin, D. C. Elias, J. A. Jaszczak, A. K. Geim, *Phys. Rev. Lett.* **2008**, 100, 016602.
- [105] X. Du, I. Skachko, A. Barker, E. Y. Andrei, *Nat. Nanotechnol.* **2008**, 3, 491.
- [106] K. I. Bolotin, K. J. Sikes, J. Hone, H. L. Stormer, P. Kim, *Phys. Rev. Lett.* **2008**, 101, 096802.
- [107] K. F. Mak, L. Ju, F. Wang, T. F. Heinz, *Solid State Commun.* **2012**, 152, 1341.
- [108] C. Casiraghi, A. Hartschuh, E. Lidorikis, H. Qian, H. Harutyunyan, T. Gokus, K. S. Novoselov, A. C. Ferrari, *Nano Lett.* **2007**, 7, 2711.
- [109] F. Wang, Y. Zhang, C. Tian, C. Girit, A. Zettl, M. Crommie, Y. R. Shen, *Science* **2008**, 320, 206.
- [110] D. K. Efetov, P. Kim, *Phys. Rev. Lett.* **2010**, 105, 256805.
- [111] C. F. Chen, C. H. Park, B. W. Boudouris, J. Horng, B. S. Geng, C. Girit, A. Zettl, M. F. Crommie, R. A. Segalman, S. G. Louie, F. Wang, *Nature* **2011**, 471, 617.
- [112] E. O. Polat, C. Kocabas, *Nano Lett.* **2013**, 13, 5851.
- [113] U. Keller, K. J. Weingarten, F. X. Kartner, D. Kopf, B. Braun, I. D. Jung, R. Fluck, C. Honninger, N. Matuschek, J. A. der Au, *IEEE J. Sel. Top. Quantum Electron.* **1996**, 2, 435.
- [114] M. Baudisch, A. Marini, J. D. Cox, T. Zhu, F. Silva, S. Teichmann, M. Massicotte, F. Koppens, L. S. Levitov, F. J. G. de Abajo, J. Biegert, *Nat. Commun.* **2018**, 9, 1018.
- [115] T. Jiang, K. Yin, C. Wang, J. You, H. Ouyang, R. Miao, C. Zhang, K. Wei, H. Li, H. Chen, R. Zhang, X. Zheng, Z. Xu, X. Cheng, H. Zhang, *Photonics Res.* **2020**, 8, 78.
- [116] A. R. Wright, X. G. Xu, J. C. Cao, C. Zhang, *Appl. Phys. Lett.* **2009**, 95, 072101.
- [117] Y. S. Ang, S. Sultan, C. Zhang, *Appl. Phys. Lett.* **2010**, 97, 243110.
- [118] E. Hendry, P. J. Hale, J. Moger, A. K. Savchenko, S. A. Mikhailov, *Phys. Rev. Lett.* **2010**, 105, 097401.
- [119] T. Gu, N. Petrone, J. F. McMillan, A. van der Zande, M. Yu, G. Q. Lo, D. L. Kwong, J. Hone, C. W. Wong, *Nat. Photonics* **2012**, 6, 554.
- [120] H. Zhang, S. Virally, Q. L. Bao, L. K. Ping, S. Massar, N. Godbout, P. Kockaert, *Opt. Lett.* **2012**, 37, 1856.
- [121] S.-Y. Hong, J. I. Dadap, N. Petrone, P.-C. Yeh, J. Hone, R. M. Osgood, *Phys. Rev. X* **2013**, 3, 021014.
- [122] J. L. Cheng, N. Vermeulen, J. E. Sipe, *New J. Phys.* **2014**, 16, 053014.
- [123] J. L. Cheng, N. Vermeulen, J. E. Sipe, *Phys. Rev. B* **2015**, 91, 235320.
- [124] K. J. A. Ooi, P. C. Leong, L. K. Ang, D. T. H. Tan, *Sci. Rep.* **2017**, 7, 12748.
- [125] X. Shao, A. Srinivasan, W. K. Ang, A. Khurshid, *Nat. Commun.* **2018**, 9, 1288.
- [126] B. Deng, P.-C. Hsu, G. Chen, B. N. Chandrashekar, L. Liao, Z. Aytimuda, J. Wu, Y. Guo, L. Lin, Y. Zhou, M. Aisijiang, Q. Xie, Y. Cui, Z. Liu, *Nano Lett.* **2015**, 15, 4206.
- [127] A. Nag, A. Mitra, *Sens. Actuators, A* **2018**, 270, 177.
- [128] R. Ismaeel, T. Lee, M. Ding, M. Belal, G. Brambilla, *Laser Photonics Rev.* **2013**, 7, 350.

- [129] J. Lou, Y. Wang, L. Tong, *Sensors* **2014**, *14*, 5823.
- [130] L. Gai, J. Li, Y. Zhao, *Opt. Laser Technol.* **2017**, *89*, 126.
- [131] G. Y. Chen, D. G. Lancaster, T. M. Monro, *Sensors* **2018**, *18*, 72.
- [132] Q. Wang, J.-Y. Jing, B.-T. Wang, S. Li, *Instrum. Sci. Technol.* **2019**, *47*, 117.
- [133] A. D. Ellis, M. E. McCarthy, M. A. Z. Al Khateeb, M. Sorokina, N. J. Doran, *Adv. Opt. Photonics* **2017**, *9*, 429.
- [134] J. Limpert, T. Schreiber, S. Nolte, H. Zellmer, A. Tunnermann, R. Iliew, F. Lederer, J. Broeng, G. Vienne, A. Petersson, C. Jakobsen, *Opt. Express* **2003**, *11*, 818.
- [135] W. J. Wadsworth, J. C. Knight, P. S. J. Russell, in *Technical Digest. Summaries of papers presented at the Conf. on Lasers and Electro-Optics. Postconference Technical Digest (IEEE Cat. No. 01CH37170)*, IEEE, Piscataway, NJ **2001**, p. 319.
- [136] T. Südmeyer, F. Brunner, E. Innerhofer, R. Paschotta, K. Furusawa, J. C. Baggett, T. M. Monro, D. J. Richardson, U. Keller, *Opt. Lett.* **2003**, *28*, 1951.
- [137] K. S. Abedin, F. Kubota, *Electron. Lett.* **2004**, *40*, 58.
- [138] P. J. Roberts, F. Couny, T. A. Birks, J. C. Knight, P. J. St Russell, B. J. Mangan, H. Sabert, D. P. Williams, L. Farr, in *Conf. on Lasers and Electro-Optics (CLEO)*, IEEE, Piscataway, NJ **2005**, Vol. 2, 1240.
- [139] J. D. Shephard, F. Couny, P. St J. Russell, J. D. C. Jones, J. C. Knight, D. P. Hand, *Appl. Opt.* **2005**, *44*, 4582.
- [140] Y. Yu, X. Li, X. Hong, Y. Deng, K. Song, Y. Geng, H. Wei, W. Tong, *Opt. Express* **2010**, *18*, 15383.
- [141] A. D. Pryamikov, A. S. Biriukov, A. F. Kosolapov, V. G. Plotnichenko, S. L. Semjonov, E. M. Dianov, *Opt. Express* **2011**, *19*, 1441.
- [142] S. Wang, S. Feng, M. Wang, C. Yu, Q. Zhou, H. Li, Y. Tang, D. Chen, L. Hu, *Laser Phys. Lett.* **2013**, *10*, 115802.
- [143] F. Poletti, *Opt. Express* **2014**, *22*, 23807.
- [144] R. Slavík, G. Marra, E. N. Fokoua, N. Baddela, N. V. Wheeler, M. Petrovich, F. Poletti, D. J. Richardson, *Sci. Rep.* **2015**, *5*, 15447.
- [145] W. Li, D. Chen, Z. Qinling, L. Hu, *Sci. Rep.* **2015**, *5*, 12547.
- [146] M. Kuschnerov, B. J. Mangan, K. Gong, V. A. J. M. Sleiffer, M. Herrmann, J. W. Nicholson, J. M. Fini, L. Meng, R. S. Windeler, E. M. Monberg, A. DeSantolo, K. Mukasa, V. Mikhailov, U. Feiste, W. Zhang, R. Yu, *J. Lightwave Technol.* **2016**, *34*, 314.
- [147] T. D. Bradley, J. R. Hayes, Y. Chen, G. T. Jasion, S. R. Sandoghchi, R. Slavik, E. N. Fokoua, S. Bawn, H. Sakr, I. A. Davidson, A. Taranta, J. P. Thomas, M. N. Petrovich, D. J. Richardson, F. Poletti, in *2018 European Conf. on Optical Communication (ECOC)*, IEEE, Rome, Italy **2018**, pp. 1–3.
- [148] E. Lee, J. Luo, B. Sun, V. L. Ramalingam, X. Yu, Q. Wang, F. Yu, J. C. Knight, in *Conf. on Lasers and Electro-Optics: Science and Innovations*, Optica Publishing Group, San Jose, CA, USA **2018**, p. SFIK.1.
- [149] Y. Tamura, H. Sakuma, K. Morita, M. Suzuki, Y. Yamamoto, K. Shimada, Y. Honma, K. Sohma, T. Fujii, T. Hasegawa, *J. Lightwave Technol.* **2018**, *36*, 44.
- [150] G. T. Jasion, T. D. Bradley, K. Harrington, H. Sakr, Y. Chen, E. N. Fokoua, I. A. Davidson, A. Taranta, J. R. Hayes, D. J. Richardson, F. Poletti, in *Optical Fiber Communication Conf. Postdeadline Papers 2020*, Optica Publishing Group, San Diego, CA, USA **2020**, p. Th4B.4.
- [151] G. T. Jasion, T. D. Bradley, H. Sakr, J. R. Hayes, Y. Chen, A. Taranta, H. C. Mulvad, I. A. Davidson, N. V. Wheeler, E. N. Fokoua, W. Wang, D. J. Richardson, F. Poletti, in *Next-Generation Optical Communication: Components, Sub-Systems, and Systems IX*, SPIE OPTO, San Francisco, CA, USA **2020**, p. 1130902.
- [152] G. T. Jasion, T. D. Bradley, K. Harrington, H. Sakr, Y. Chen, E. N. Fokoua, I. A. Davidson, A. Taranta, J. R. Hayes, D. J. Richardson, F. Poletti, in *2021 Optical Fiber Communication Conf. (OFC)*, Optica Publishing Group, Washington, DC, USA **2021**, p. M5E.2.
- [153] W. Chang, A. Nazarkin, J. C. Travers, J. Nold, P. Holzer, N. Y. Joly, P. S. J. Russell, *Opt. Express* **2011**, *19*, 21018.
- [154] M. F. Saleh, W. Chang, J. C. Travers, P. St J. Russell, F. Biancalana, *Phys. Rev. Lett.* **2012**, *109*, 113902.
- [155] K. F. Mak, J. C. Travers, P. Holzer, N. Y. Joly, P. S. Russell, *Opt. Express* **2013**, *21*, 10942.
- [156] M. Azhar, N. Y. Joly, J. C. Travers, P. S. Russell, *Appl. Phys. B: Lasers Opt.* **2013**, *112*, 457.
- [157] M. Azhar, G. K. L. Wong, W. Chang, N. Y. Joly, P. J. Russell, *Opt. Express* **2013**, *21*, 4405.
- [158] P. Vaiano, B. Carotenuto, M. Pisco, A. Ricciardi, G. Quero, M. Consoles, A. Crescitelli, E. Esposito, A. Cusano, *Laser Photonics Rev.* **2016**, *10*, 922.
- [159] L. Scolari, S. Gauza, H. Q. Xianyu, L. Zhai, L. Eskildsen, T. T. Alkeskjold, S. T. Wu, A. Bjarklev, *Opt. Express* **2009**, *17*, 3754.
- [160] R. R. He, P. J. A. Sazio, A. C. Peacock, N. Healy, J. R. Sparks, M. Krishnamurthi, V. Gopalan, J. V. Badding, *Nat. Photonics* **2012**, *6*, 174.
- [161] H. W. Lee, M. A. Schmidt, H. K. Tyagi, L. P. Sempere, P. St J. Russell, *Appl. Phys. Lett.* **2008**, *93*, 111102.
- [162] S. Zhang, J. Li, S. Li, Q. Liu, Y. Liu, Z. Zhang, Y. Wang, *Appl. Phys. B* **2018**, *124*, 112.
- [163] Md. N. Hossen, Md. Ferdous, K. Ahmed, Md. A. Khalek, S. Chakma, B. K. Paul, *Front. Optoelectron.* **2019**, *12*, 157.
- [164] C. Liu, J. W. Lu, W. Liu, F. M. Wang, P. K. Chu, *Chin. Opt. Lett.* **2021**, *19*, 102202.
- [165] Q. L. Bao, H. Zhang, B. Wang, Z. H. Ni, C. H. Y. X. Lim, Y. Wang, D. Y. Tang, K. P. Loh, *Nat. Photonics* **2011**, *5*, 411.
- [166] Y.-W. Song, S.-Y. Jang, W.-S. Han, M.-K. Bae, *Appl. Phys. Lett.* **2010**, *96*, 051122.
- [167] S. Y. Choi, D. K. Cho, Y.-W. Song, K. Oh, K. Kim, F. Rotermund, *Opt. Express* **2012**, *20*, 5652.
- [168] J. Zhao, S. Ruan, P. Yan, H. Zhang, Y. Yu, H. Wei, J. Luo, *Opt. Eng.* **2013**, *52*, 106105.
- [169] Y. H. Lin, C. Y. Yang, J. H. Liou, C. P. Yu, G. R. Lin, *Opt. Express* **2013**, *21*, 16763.
- [170] W. Li, B. G. Chen, C. Meng, W. Fang, Y. Xiao, X. Y. Li, Z. F. Hu, Y. X. Xu, L. M. Tong, H. Q. Wang, W. T. Liu, J. M. Bao, Y. R. Shen, *Nano Lett.* **2014**, *14*, 955.
- [171] S. J. Tan, H. Haris, X. S. Cheng, S. W. Harun, in *2019 18th Int. Conf. on Optical Communications and Networks (ICOON)*, IEEE, Huangshan, China **2019**, pp. 1–3.
- [172] F. Zhou, W. Du, *Appl. Opt.* **2018**, *57*, 6645.
- [173] Y. Zhao, X.-g. Li, X. Zhou, Y.-n. Zhang, *Sens. Actuators, B* **2016**, *231*, 324.
- [174] D. Popa, Z. Sun, F. Torrisi, T. Hasan, F. Wang, A. C. Ferrari, *Appl. Phys. Lett.* **2010**, *97*, 203106.
- [175] Y. Zuo, W. Yu, C. Liu, X. Cheng, R. Qiao, J. Liang, X. Zhou, J. Wang, M. Wu, Y. Zhao, P. Gao, S. Wu, Z. Sun, K. Liu, X. Bai, Z. Liu, *Nat. Nanotechnol.* **2020**, *15*, 987.
- [176] M. Marchena, F. Wagner, T. Arluigie, B. Zhu, B. Johnson, M. Fernández, T. L. Chen, T. Chang, R. Lee, V. Pruneri, P. Mazumder, *2D Mater.* **2018**, *5*, 035022.
- [177] Y. Song, W. Zou, Q. Lu, L. Lin, Z. Liu, *Small* **2021**, *17*, 2007600.
- [178] Y. P. Hsieh, C. H. Shih, Y. J. Chiu, M. Hofmann, *Chem. Mater.* **2016**, *28*, 40.
- [179] H. Wang, X. Xu, J. Li, L. Lin, L. Sun, X. Sun, S. Zhao, C. Tan, C. Chen, W. Dang, H. Ren, J. Zhang, B. Deng, A. L. Koh, L. Liao, N. Kang, Y. Chen, H. Xu, F. Ding, K. Liu, H. Peng, Z. Liu, *Adv. Mater.* **2016**, *28*, 8968.
- [180] J. Xu, J. Hu, Q. Li, R. Wang, W. Li, Y. Guo, Y. Zhu, F. Liu, Z. Ullah, G. Dong, Z. Zeng, L. Liu, *Small* **2017**, *13*, 1700651.
- [181] Y. Li, L. Sun, Z. Chang, H. Liu, Y. Wang, Y. Liang, B. Chen, Q. Ding, Z. Zhao, R. Wang, Y. Wei, H. Peng, L. Lin, Z. Liu, *Adv. Mater.* **2020**, *32*, 2002034.
- [182] Y. Zhang, D. Huang, Y. Duan, H. Chen, L. Tang, M. Shi, Z. Li, H. Shi, *Nanotechnology* **2020**, *32*, 105603.

- [183] B. Sun, J. Pang, Q. Cheng, S. Zhang, Y. Li, C. Zhang, D. Sun, B. Ibarlucea, Y. Li, D. Chen, H. Fan, Q. Han, M. Chao, H. Liu, J. Wang, G. Cuniberti, L. Han, W. Zhou, *Adv. Mater. Technol.* **2021**, 6, 2000744.
- [184] K. Jia, J. Zhang, Y. Zhu, L. Sun, L. Lin, Z. Liu, *Appl. Phys. Rev.* **2021**, 8, 041306.
- [185] Y. Wang, F. Qing, Y. Jia, Y. Duan, C. Shen, Y. Hou, Y. Niu, H. Shi, X. Li, *Chem. Eng. J.* **2021**, 405, 127014.
- [186] J. Y. Chen, Y. G. Wen, Y. L. Guo, B. Wu, L. P. Huang, Y. Z. Xue, D. C. Geng, D. Wang, G. Yu, Y. Q. Liu, *J. Am. Chem. Soc.* **2011**, 133, 17548.
- [187] J. Y. Chen, Y. L. Guo, Y. G. Wen, L. P. Huang, Y. Z. Xue, D. C. Geng, B. Wu, B. R. Luo, G. Yu, Y. Q. Liu, *Adv. Mater.* **2013**, 25, 992.
- [188] D. Wei, Y. Lu, C. Han, T. Niu, W. Chen, *Angew. Chem., Int. Ed.* **2013**, 52, 14121.
- [189] J. Y. Chen, Y. L. Guo, L. L. Jiang, Z. P. Xu, L. P. Huang, Y. Z. Xue, D. C. Geng, B. Wu, W. P. Hu, G. Yu, Y. Q. Liu, *Adv. Mater.* **2014**, 26, 1348.
- [190] J. Y. Sun, Y. B. Chen, M. K. Priyadarshi, Z. Chen, A. Bachmatiuk, Z. Y. Zou, Z. L. Chen, X. J. Song, Y. F. Gao, M. H. Rummeli, Y. F. Zhang, Z. F. Liu, *Nano Lett.* **2015**, 15, 5846.
- [191] Y. B. Chen, J. Y. Sun, J. F. Gao, F. Du, Q. Han, Y. F. Nie, Z. Chen, A. Bachmatiuk, M. K. Priyadarshi, D. L. Ma, X. J. Song, X. S. Wu, C. Y. Xiong, M. H. Rummeli, F. Ding, Y. F. Zhang, Z. F. Liu, *Adv. Mater.* **2015**, 27, 7839.
- [192] J. Y. Sun, Y. B. Chen, M. K. Priyadarshi, T. Gao, X. J. Song, Y. F. Zhang, Z. F. Liu, *Adv. Mater.* **2016**, 28, 10333.
- [193] X.-D. Chen, Z. Chen, W.-S. Jiang, C. Zhang, J. Sun, H. Wang, W. Xin, L. Lin, M. K. Priyadarshi, H. Yang, Z.-B. Liu, J.-G. Tian, Y. Zhang, Y. Zhang, Z. Liu, *Adv. Mater.* **2017**, 29, 1603428.
- [194] Z. Chen, Y. Qi, X. Chen, Y. Zhang, Z. Liu, *Adv. Mater.* **2019**, 31, 1803639.
- [195] G. Cui, Y. Cheng, C. Liu, K. W. Huang, J. L. Li, P. X. Wang, X. J. Duan, K. Chen, K. H. Liu, Z. F. Liu, *ACS Nano* **2020**, 14, 5938.
- [196] H. Yuan, H. Zhang, K. Huang, Y. Cheng, K. Wang, S. Cheng, W. Li, J. Jiang, J. Li, C. Tu, X. Wang, Y. Qi, Z. Liu, *ACS Nano* **2022**, 16, 2577.
- [197] S. Bhaviripudi, X. Jia, M. S. Dresselhaus, J. Kong, *Nano Lett.* **2010**, 10, 4128.
- [198] G. Li, S.-H. Huang, Z. Li, *Phys. Chem. Chem. Phys.* **2015**, 17, 22832.
- [199] B. Hou, R. Xiang, T. Inoue, E. Einarsson, S. Chiashi, J. Shiomi, A. Miyoshi, S. Maruyama, *Jpn. J. Appl. Phys.* **2011**, 50, 065101.
- [200] R. Xiang, B. Hou, E. Einarsson, P. Zhao, S. Harish, K. Morimoto, Y. Miyauchi, S. Chiashi, *ACS Nano* **2013**, 7, 3095.
- [201] M. H. Rummeli, A. Bachmatiuk, A. Scott, F. Börrnert, J. H. Warner, V. Hoffmann, J.-H. Lin, G. Cuniberti, B. Büchner, *ACS Nano* **2010**, 4, 4206.
- [202] K.-B. Kim, C.-M. Lee, J. Choi, *J. Phys. Chem. C* **2011**, 115, 14488.
- [203] Y. Miyasaka, A. Nakamura, J. Temmyo, *Jpn. J. Appl. Phys.* **2011**, 50, 04DH12.
- [204] E. J. Lee, S. Y. Choi, H. Jeong, N. H. Park, W. Yim, M. H. Kim, J.-K. Park, S. Son, S. Bae, S. J. Kim, K. Lee, Y. H. Ahn, K. J. Ahn, B. H. Hong, J.-Y. Park, F. Rotermund, *Nat. Commun.* **2015**, 6, 6851.
- [205] H. Zhang, N. Healy, L. Shen, C. C. Huang, N. Aspiotis, D. W. Hewak, A. C. Peacock, *J. Lightwave Technol.* **2016**, 34, 3563.
- [206] X. Liu, L. Yang, J. Ma, C. Li, W. Jin, W. Bi, *Chin. Phys. B* **2018**, 27, 104206.
- [207] S. Zhang, Z. Li, F. Xing, *Int. J. Mol. Sci.* **2020**, 21, 1608.
- [208] Q. Bao, H. Zhang, Z. Ni, Y. Wang, L. Polavarapu, Z. Shen, Q.-H. Xu, D. Tang, *Nano Res.* **2011**, 4, 297.
- [209] B. C. Yao, Y. J. Rao, S. W. Huang, Y. Wu, Z. Y. Feng, C. Choi, H. Liu, H. F. Qi, X. F. Duan, G. D. Peng, C. W. Wong, *Opt. Express* **2017**, 25, 8202.
- [210] D. Li, H. Xue, M. Qi, Y. Wang, S. Aksimsek, N. Chekurov, W. Kim, C. Li, J. Riikonen, F. Ye, Q. Dai, Z. Ren, J. Bai, T. Hasan, H. Lipsanen, Z. Sun, *2D Mater.* **2017**, 4, 025095.
- [211] G. Sobon, P. R. Kaczmarek, D. Sliwiska, J. Sotor, K. M. Abramski, *IEEE J. Sel. Top. Quantum Electron.* **2014**, 20, 492.
- [212] M. Liu, R. Tang, A.-P. Luo, W.-C. Xu, Z.-C. Luo, *Photonics Res.* **2018**, 6, C1.
- [213] Z. Luo, M. Zhou, J. Weng, G. Huang, H. Xu, C. Ye, Z. Cai, *Opt. Lett.* **2010**, 35, 3709.
- [214] A. Ren, M. Feng, F. Song, Y. Ren, S. Yang, Z. Yang, Y. Li, Z. Liu, J. Tian, *Opt. Express* **2015**, 23, 21490.
- [215] W. Liu, M. Liu, X. Liu, X. Wang, H.-X. Deng, M. Lei, Z. Wei, Z. Wei, *Adv. Opt. Mater.* **2020**, 8, 1901631.
- [216] M. Chhowalla, D. Jena, H. Zhang, *Nat. Rev. Mater.* **2016**, 1, 16052.
- [217] X. Cheng, X. Zhou, L. Tao, W. Yu, C. Liu, Y. Cheng, C. Ma, N. Shang, J. Xie, K. Liu, Z. Liu, *Nanoscale* **2020**, 12, 14472.
- [218] W. Yang, G. Chen, Z. Shi, C.-C. Liu, L. Zhang, G. Xie, M. Cheng, D. Wang, R. Yang, D. Shi, K. Watanabe, T. Taniguchi, Y. Yao, Y. Zhang, G. Zhang, *Nat. Mater.* **2013**, 12, 792.
- [219] X. Wang, G. Fu, Y. Cui, X. Fu, W. Jin, W. Bi, *Appl. Phys. Express* **2020**, 13, 102006.
- [220] X. Cheng, X. Zhou, C. Huang, C. Liu, C. Ma, H. Hong, W. Yu, K. Liu, Z. Liu, *Chin. Phys. B* **2021**, 30, 118103.
- [221] F. Liao, J. Yu, Z. Gu, Z. Yang, T. Hasan, S. Linghu, J. Peng, W. Fang, S. Zhuang, M. Gu, F. Gu, *Sci. Adv.* **2019**, 5, eaax7398.
- [222] A. Lewis, F. De Lucia, W. Belardi, C. C. Huang, J. Hayes, F. Poletti, D. Hewak, P. J. Sazio, in *Optical Components and Materials XVII*, SPIE OPTO, San Francisco, CA, USA **2020**, p. 1127608.
- [223] G. Q. Ngo, A. George, R. T. K. Schock, A. Tuniz, E. Najafidehaghani, Z. Gan, N. C. Geib, T. Bucher, H. Knopf, S. Saravi, C. Neumann, T. Lühder, E. P. Schartner, S. C. Warren-Smith, H. Ebdorff-Heidepriem, T. Pertsch, M. A. Schmidt, A. Turchanin, F. Eilenberger, *Adv. Mater.* **2020**, 32, 2003826.
- [224] S. Dai, Q. Ma, M. K. Liu, T. Andersen, Z. Fei, M. D. Goldflam, M. Wagner, K. Watanabe, T. Taniguchi, M. Thiemens, F. Keilmann, G. C. A. M. Janssen, S. E. Zhu, P. Jarillo-Herrero, M. M. Fogler, D. N. Basov, *Nat. Nanotechnol.* **2015**, 10, 682.
- [225] H. Yao, X. Guo, A. Bao, H. Mao, Y. Ma, X. Li, *Chin. Phys. B* **2022**, 31, 038501.



Xu Zhou is currently an associate professor at the School of Physics and Telecommunication Engineering, South China Normal University, China. He received his B.S. degree from Northwestern Polytechnical University in 2014 and his Ph.D. degree from Peking University in 2018, followed by his postdoctoral research in Peking University until 2020. His research interests mainly focus on the spectral physics and device physics of 2D materials and the hybrid 2D materials-optical fibers.



Qingyan Deng is currently a master research fellow at the School of Physics and Telecommunication Engineering, South China Normal University, China. He received his B.S. degree from South China Normal University in 2019. His research interests mainly focus on the spectral physics and device physics of 2D materials and the hybrid 2D materials-optical fibers.



Wentao Yu is currently a professor at Institute of Interdisciplinary Physical Sciences, School of Science, Nanjing University of Science and Technology, China. He received his B.S. degree from Southeast University in 2012 and his Ph.D. degree from Peking University in 2017, followed by his postdoctoral research in Peking University until 2021. His research interests mainly focus on the optical microscope, optical spectra, and nonlinear optics of 2D materials and the hybrid 2D materials-optical fibers.



Kaihui Liu is currently a full professor and principle-investigator in the State Key Lab for Mesoscopic Physics, School of Physics, Peking University, China. He received his Ph.D. from the Institute of Physics, Chinese Academy of Sciences in 2009 and afterward worked as a postdoctoral research fellow at UC Berkeley, USA, until 2014. His current research interests are the growth, characterization, and applications of meter-scale single crystals including single-crystal copper foil, graphene, TMDCs, and graphene-fiber.



Zhongfan Liu is currently a full professor and principle-investigator in the Beijing National Laboratory for Molecular Sciences, College of Chemistry and Molecular Engineering, Peking University, China. He is also the director of Beijing Graphene Institute in China. He was elected as the member of Chinese Academy of Sciences in 2011. He received his Ph.D. from University of Tokyo in 1990, and afterward worked as a postdoctoral fellowship at the Institute for Molecular Science, Japan, until 1993. His research interest focusses on low dimensional carbon materials, including the CVD growth of graphene and single-walled carbon nanotubes and their unique applications.